cAMP-dependent regulation of I_{Ks} single-channel kinetics

Emely Thompson,[1] Jodene Eldstrom,[1] Maartje Westhoff,[1] Donald McAfee,[1] Elise Balse,[2] and David Fedida[1]

[1]Department of Anesthesiology, Pharmacology, and Therapeutics, University of British Columbia, Vancouver, BC, Canada
[2]Sorbonne Universités, UPMC Univ Paris 06, INSERM, UMR_S 1166, Unité de recherche sur les maladies cardiovasculaires, le métabolisme et la nutrition, Faculté de Médecine, Site Pitié-Salpêtrière, Paris, France

The delayed potassium rectifier current, I_{Ks}, is composed of KCNQ1 and KCNE1 subunits and plays an important role in cardiac action potential repolarization. During β-adrenergic stimulation, 3′-5′-cyclic adenosine monophosphate (cAMP)-dependent protein kinase A (PKA) phosphorylates KCNQ1, producing an increase in I_{Ks} current and a shortening of the action potential. Here, using cell-attached macropatches and single-channel recordings, we investigate the microscopic mechanisms underlying the cAMP-dependent increase in I_{Ks} current. A membrane-permeable cAMP analog, 8-(4-chlorophenylthio)-cAMP (8-CPT-cAMP), causes a marked leftward shift of the conductance–voltage relation in macropatches, with or without an increase in current size. Single channels exhibit fewer silent sweeps, reduced first latency to opening (control, 1.61 ± 0.13 s; cAMP, 1.06 ± 0.11 s), and increased higher-subconductance-level occupancy in the presence of cAMP. The E160R/R237E and S209F KCNQ1 mutants, which show fixed and enhanced voltage sensor activation, respectively, largely abolish the effect of cAMP. The phosphomimetic KCNQ1 mutations, S27D and S27D/S92D, are much less and not at all responsive, respectively, to the effects of PKA phosphorylation (first latency of S27D + KCNE1 channels: control, 1.81 ± 0.1 s; 8-CPT-cAMP, 1.44 ± 0.1 s, $P < 0.05$; latency of S27D/S92D + KCNE1: control, 1.62 ± 0.1 s; cAMP, 1.43 ± 0.1 s, nonsignificant). Using total internal reflection fluorescence microscopy, we find no overall increase in surface expression of the channel during exposure to 8-CPT-cAMP. Our data suggest that the cAMP-dependent increase in I_{Ks} current is caused by an increase in the likelihood of channel opening, combined with faster openings and greater occupancy of higher subconductance levels, and is mediated by enhanced voltage sensor activation.

INTRODUCTION

The repolarization phase of the cardiac action potential is dominated by the activity of two K^+ currents, I_{Ks} and I_{Kr} (Sanguinetti and Jurkiewicz, 1990). At normal heart rates, I_{Ks} plays the lesser role, but at high heart rates and during stress, the current is up-regulated and the rate of deactivation is slowed (Terrenoire et al., 2005). This increase in I_{Ks} leads to a repolarization reserve, which shortens the action potential duration and allows for adequate ventricular filling (Stengl et al., 2003; Jost et al., 2005; Silva and Rudy, 2005).

I_{Ks} is the product of the coassembly of the $K_v7.1$ voltage-gated potassium channel (KCNQ1 [Q1]) with the KCNE1 (E1) β-subunit. The coassembly of E1 with Q1 causes notable changes in channel kinetics, converting a rapidly activating current into one with very slow activation and deactivation kinetics, and in which inactivation is altogether abolished. In addition, overall current amplitude is increased upon E1 coassembly (Takumi et al., 1988; Barhanin et al., 1996; Sanguinetti et al., 1996; Tristani-Firouzi and Sanguinetti, 1998). Mutations in Q1 or E1 can cause cardiac arrhythmias such as long QT and short QT syndromes and familial atrial fibrillation (Moss et al., 1991; Chen et al., 2003; Bellocq et al., 2004). Long QT mutations lead to a lengthening of the action potential because the amount of repolarizing I_{Ks} is reduced (Wang et al., 1996; Splawski et al., 2000). Because of the importance of I_{Ks} at high heart rates, many individuals with these mutations display symptoms when their heart rates are elevated—for example, while exercising or when under stress (Wit et al., 1975).

Response to stressful situations—for example, fight or flight—involves sympathetic nervous system activation via β-adrenergic receptors (β-ARs). This triggers a signaling cascade, which leads to phosphorylation of Q1 and an increase in I_{Ks} current. The β-ARs are coupled to heterotrimeric G-proteins that release GTP-bound α-subunits to activate the downstream effector, adenylyl cyclase 9 (Cumbay and Watts, 2004; Piggott et al., 2008; Dessauer, 2009). Activating adenylyl cyclase 9 increases the level of intracellular cAMP, which in turn activates cAMP-dependent protein kinase A (PKA). PKA is brought into the macromolecular complex and in close proximity to Q1 by Yotiao (A-kinase anchoring protein 9 [AKAP-9]), which allows PKA to phosphorylate the residue Ser^{27} (Fig. 1; Chen et al., 2005; Piggott et al., 2008; Li et al., 2012). Yotiao also anchors protein phosphatase 1 (PP1), which is key for regulation of β-AR stimulation of I_{Ks} (Fig. 1; Marx et al., 2002).

Correspondence to David Fedida: david.fedida@ubc.ca

Abbreviations used: β-AR, β-adrenergic receptor; OA, okadaic acid; Po, open probability; ROI, region of interest; TIRF, total internal reflection fluorescence; VSD, voltage sensor domain.

The Rockefeller University Press
J. Gen. Physiol. Vol. 149 No. 8 781–798
https://doi.org/10.1085/jgp.201611734

The Journal of General Physiology

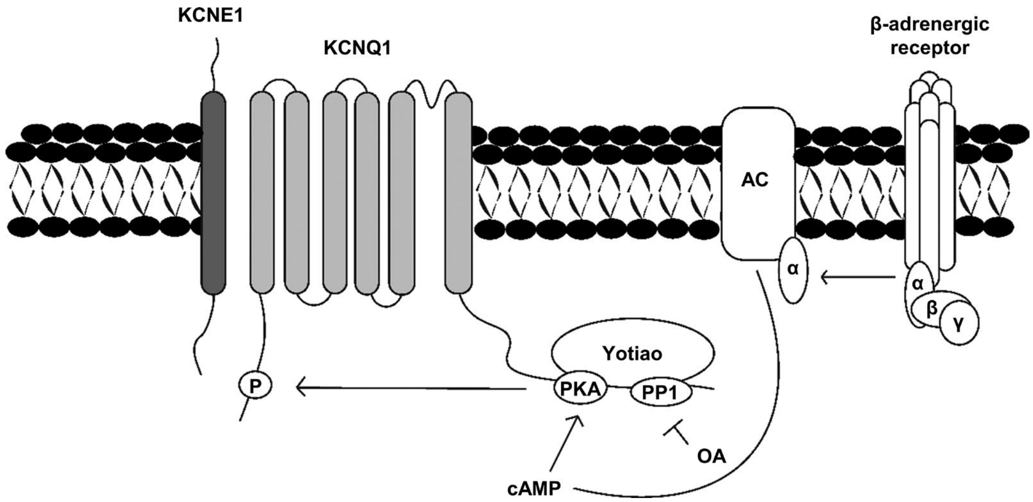

Figure 1. **Phosphorylation of I_{Ks} by PKA.** Once the G protein–coupled β-adrenergic receptor is activated, GTP binds to the α-subunit of the G protein, which allows for the release of active α-GTP subunits. This complex binds and activates adenylyl cyclase (AC), producing cAMP, which activates cAMP-dependent PKA. Yotiao anchors PKA to the KCNQ1 channel, which allows the activated PKA to phosphorylate the N terminus of the KCNQ1 channel. Protein phosphatase 1 can dephosphorylate cAMP-mediated phosphorylation and is blocked by OA.

The full range of mechanisms behind the increase in I_{Ks} current after β-adrenergic stimulation is not fully understood. Phosphorylation of channels is known to cause a hyperpolarizing shift of the half-activation potential ($V_{1/2}$), where the I_{Ks} channels open at more negative membrane potentials (Dilly et al., 2004; Terrenoire et al., 2005). Along with this is an increase in the rate of activation and a decrease in the rate of deactivation (Terrenoire et al., 2005), which increases I_{Ks} by allowing a buildup of open channels during successive depolarizations. As well, increases in current could be caused by a change in the number of channels at the cell surface. This has been seen to be the case for other ion transporters, such as the Na^+/K^+-ATPase pump, which shows increased translocation to the plasma membrane during cAMP stimulation (Gonin et al., 2001).

Here, we aimed to study the mechanisms by which β-adrenergic stimulation increases the I_{Ks} current at the microscopic ion channel level. From our prior work, we now understand that I_{Ks} channels do not occupy a single open state but transition through five or six open levels during activation of the channel complex, and only reach an open probability (Po) of ∼0.15–0.2 at 60 mV, even during prolonged depolarizations (Werry et al., 2013; Eldstrom et al., 2015; Murray et al., 2016). Once current reaches a stable level, channel activity is characterized by preferential occupancy of two or three relatively higher subconductance states while the channel pore opens in long bursts with frequent brief closings. By using a membrane-permeant cAMP analog, 8-CPT-cAMP, we can look for modulation of the single-channel kinetics in cell-attached patches. Up-regulation of voltage sensor domain (VSD) function is expected to cause changes in the first latency to opening or an increased Po that would underlie reported whole-cell findings such as the hyperpolarizing shift of the conductance–voltage (G-V) relationship. In addition, we hypothesize that PKA phosphorylation can facilitate single-channel gating and induce changes in substate occupancy that further increase single-channel currents.

MATERIALS AND METHODS

Reagents

To activate PKA inside cells, membrane-permeable cAMP was used in the form of 8-(4-chlorophenylthio)adenosine 3′,5′-cyclic monophosphate sodium salt (Sigma-Aldrich). To maintain activation of PKA after stimulation, okadaic acid (OA) was used to inhibit PP1 and PP2A phosphatases (EMD Millipore). To ensure that channels under study were indeed I_{Ks}, chromanol 293B was used as a selective blocker (Tocris Bioscience).

Molecular biology

KCNQ1 and KCNE1 constructs were bought from OriGene. Throughout the article, Q1 and E1 are used as abbreviations for KCNQ1 and KCNE1, respectively. Q1 S209F was constructed from the KCNQ1 gene using a two-step PCR reaction (Eldstrom et al., 2010). Q1 S27D was a gift from the laboratory of N. Schmitt of the University of Copenhagen (Copenhagen, Denmark). Yotiao (AKAP-9) was a gift of R. Kass of Columbia University (New York, NY) and was inserted into a pcDNA3 vector. The E160R/R237E (E1R/R4E) and S27D/S92D KCNQ1 mutants were gifts from J. Cui of Washington University (St. Louis, MO). The EQ construct forces a 4:4 KCNQ1:KCNE1 stoichiometry to I_{Ks} and was constructed by tethering the C terminus

FLAG tag on KCNE1 and a V5 epitope on KCNQ1, plus an additional 21 aa (SRGGSGGSGGSGGSGGSGGRS) after the FLAG-tag sequence (Murray et al., 2016). Sequencing confirmed all mutations.

Cell culture and transfections

For single-channel recordings, Itk⁻ mouse fibroblast (LM) cells were used. They were plated to a confluence of 10–20% on sterile glass coverslips. These cells were transfected using Lipofectamine 2000 (Thermo Fisher Scientific) and with DNA ratios of 1:3:1.5:1 of KCNQ1, KCNQ1-S209F, KCNQ1-S27D, or KCNQ1-S27D/S92D :KCNE1:AKAP-9:GFP. For some experiments, E1-GFP was used to reduce the number of transfected plasmids. The cells were grown in MEM with 10% FBS (Gibco) and incubated in air/5% CO_2 at 37°C. All recordings were done at room temperature, 24–48 h posttransfection.

For total internal reflection fluorescence (TIRF) microscopy, Chinese hamster ovary (CHO) cells were grown in DMEM/F12 (Thermo Fisher Scientific) supplemented with 10% FBS, 100 IU/ml penicillin, and 100 µg/ml streptomycin (Thermo Fisher Scientific). Cells were cultured at 37°C in an air/5% CO_2 incubator. 1 d before transfection, cells were rinsed with 1× PBS (Thermo Fisher Scientific), lifted via 3-min exposure to trypsin-EDTA (Thermo Fisher Scientific), and replated on 35-mm^2 glass-bottom microdishes (Ibidi). The cells were transiently transfected using Lipofectamine 2000 according to the manufacturer's protocol. KCNE1-mCherry was coexpressed with KCNQ1-GFP and AKAP-9 in a 4:1:1 ratio. Cells were imaged 24–48 h after transfection.

Patch-clamp electrophysiology

Methods for single-channel recordings were previously published (Werry et al., 2013; Eldstrom et al., 2015). Whole-cell recordings were performed and patch electrodes were fabricated as previously described (Murray et al., 2016). Data were collected and analyzed using Axopatch hardware and pCLAMP 10.5 software (Molecular Devices).

Microscopy

I_{Ks} channels in CHO cells were visualized at ~27°C with TIRF microscopy as described previously (Boycott et al., 2013). Cells were imaged for 15 or 30 min, with 200 µM 8-CPT-cAMP added to the bath after 5 or 15 min, respectively.

Solutions

For single-channel recordings, the solution in the bath contained 135 mM KCl, 1 mM $MgCl_2$, 1 mM $CaCl_2$, and 10 mM Hepes and was adjusted to pH 7.4 with KOH. The solution in the patch pipette contained 6 mM NaCl, 129 mM MES, 1 mM $MgCl_2$, 10 mM Hepes, 5 mM KCl, and 1 mM $CaCl_2$ and was adjusted to pH 7.4 with NaOH. For whole-cell recordings, the solution in the bath contained 135 mM NaCl, 5 mM KCl, 1 mM $MgCl_2$, 2.8 mM NaAcetate, and 10 mM Hepes, pH adjusted to 7.4 with NaOH. The solution in the pipette contained 130 mM KCl, 5 mM EGTA, 1 mM $MgCl_2$, 4 mM Na_2-ATP, 0.1 mM GTP, and 10 mM Hepes, pH adjusted to 7.2 with KOH. For TIRF microscopy, the external solution contained 135 mM NaCl, 4 mM KCl, 2 mM $MgCl_2$, 2.5 mM Na-pyruvate, 1 mM Na_2HPO_4, 20 mM D-glucose, and 10 mM Hepes, pH adjusted to 7.4 with NaOH.

Data analysis

For TIRF microscopy imaging, overall fluorescence intensity of the cells was measured using Xcellence software (Olympus). Fluorescence of specific regions of interest (ROIs) was quantified using ImageJ with the Time Series Analyzer v3 plugin (National Institutes of Health).

G-V relations were acquired from normalized tail current amplitudes. Fitting the data from each cell with a Boltzmann sigmoidal function allowed us to obtain the $V_{1/2}$ values. Data analysis was done using Prism 7 (GraphPad Software). Single-channel current records were acquired at 2 kHz and digitized using Digidata 1440A hardware (Molecular Devices). For presentation and for all-points histograms (unless otherwise stated), data were filtered at 200 Hz. To compile events lists, data were filtered at 500 Hz and idealized using the Single-Channel Search function in Clampfit. Cursors were set between capacity transients at the beginning and end of the test pulse. Levels were set to 0, 0.145, 0.22, 0.33, 0.5, and 0.75 pA, and the "update level automatically" function was disabled. The program automatically detects each event and is then added to the events worksheet from which idealized amplitudes can be extracted. The final mean amplitudes of events at each sublevel are returned by the program (see legend to Fig. 5). Only events longer than 1.5 ms in duration were used in the analysis. A short section of current idealization shown in Fig. S8 B.

Statistics

Results reported here are expressed as mean ± SE and represent data from at least three independent experiments. The median value and 95% confidence intervals are also reported for first-latency data. To compare control and cAMP-treated cells, nonparametric Mann–Whitney test was used (GraphPad Software). The statistically significant threshold was set at 0.05 or less. Gaussian fits and single-channel analysis were performed using Clampfit. Nonlinear regressions were used on G-V relations using the Boltzmann sigmoidal function in Prism 7.

Online supplemental material

Figs. S1 and S2 show Q1 + E1 single-channel data before and after cAMP. Fig. S3 shows $V_{1/2}$ changes in macro-

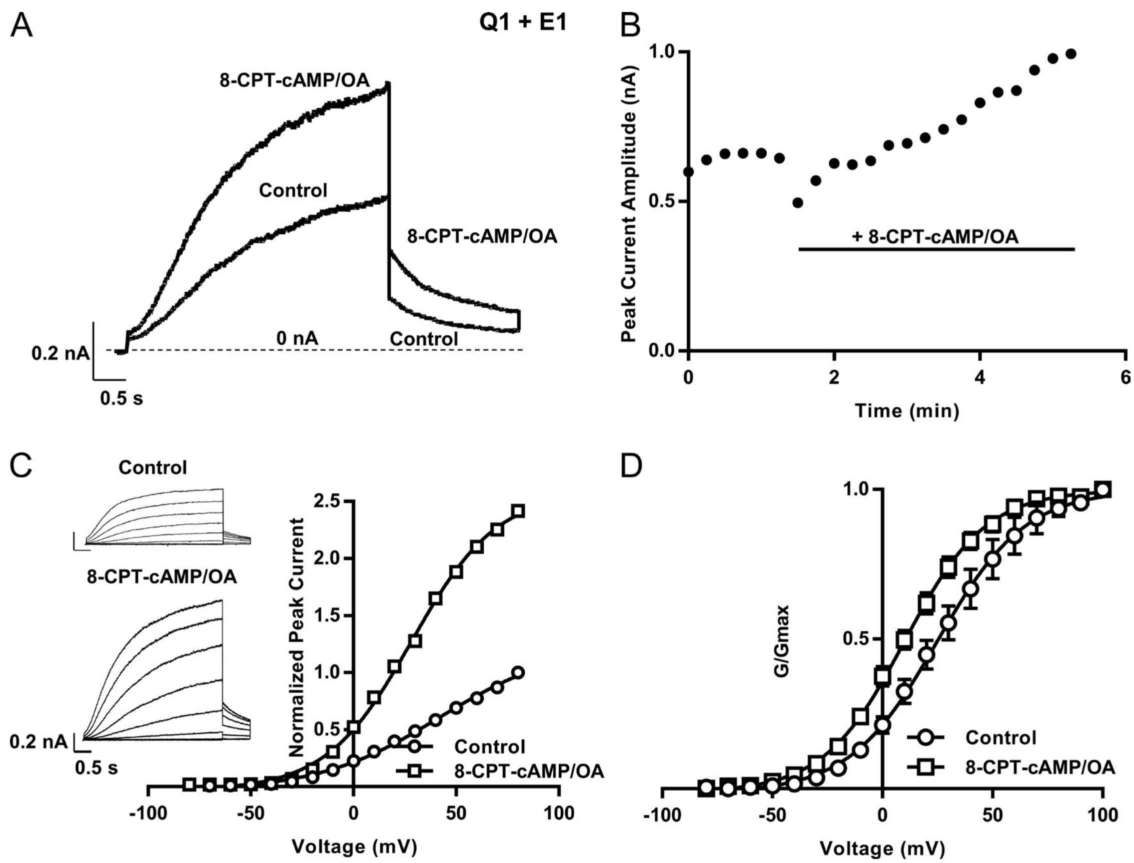

Figure 2. **Increase in whole-cell I_{Ks} current at room temperature after 8-CPT-cAMP addition.** (A) Representative traces of Q1+E1 and Yotiao before (control) and after 8-CPT-cAMP (200 µM) + OA (0.2 µM). Cells were held at −80 mV and then pulsed to 60 mV for 4 s before being pulsed to −40 mV for 2 s. (B) Diary plot of the peak outward current during a 4-s pulse to 60 mV over time (same protocol as in A). Bar indicates the addition of 200 µM 8-CPT-cAMP/0.2 µM OA to the bath. (C) I-V current traces and their peak amplitude plotted against voltage (*n* = 1) before and after 8-CPT-cAMP. Cells were held at −90 mV and pulsed from −80 mV to 100 mV in 10-mV steps for 4 s. Tail currents were recorded at −40 mV for 900 ms. Representative traces are shown from every other voltage. (D) G-V curves before ($V_{1/2}$ = 28.2 ± 5.4 mV) and after ($V_{1/2}$ = 10.5 ± 2.6 mV) 8-CPT-cAMP; *n* = 4. Error bars show ±SE.

patches before and after cAMP of EQ and S27D + E1. Figs. S4 and S5 show a detailed subconductance and kinetic analysis of S27D + E1. Fig. S6 shows whole-cell data of S209F + E1 before and after cAMP. Fig. S7 shows further analysis of the TIRF data focusing on ROIs and how those change after cAMP addition. Fig. S8 shows a snapshot of the idealization process used for subconductance analysis in Fig. 5 and Fig. S4.

RESULTS

The 8-CPT-cAMP–induced increase in I_{Ks} current is seen at room temperature

It is not possible to resolve the kinetics of single-channel I_{Ks} currents at 37°C because of the rapid shifts between subconductance levels and the need to keep noise levels extremely low. Thus, experiments were done at room temperature (20–22°C). To confirm that the expected β-adrenergic modulation of I_{Ks} was still present at these temperatures in our hands, we first used whole-cell recording to look at the effect of 8-CPT-cAMP on macroscopic I_{Ks} currents.

Q1 was transiently transfected with E1 and Yotiao into a mouse fibroblast cell line, and whole-cell currents were recorded (Fig. 2). Representative currents during a 4-s pulse to 60 mV before (control) and after 200 µM 8-CPT-cAMP (Fig. 2 A) show that I_{Ks} increased significantly even at room temperature. The time course of the increase in peak current is illustrated in the diary plot (Fig. 2 B). There was an initial decrease in current as the 8-CPT-cAMP was added to the bath, and then a delayed onset as it permeated across the membrane, followed by a progressive increase in current amplitude.

The characteristic sigmoidal shape of I_{Ks} current activation is shown in the representative traces in Fig. 2. Apart from the increased current size apparent in the current–voltage (I-V) relationship (Fig. 2 C), the mean G-V curve (Fig. 2 D), obtained from analysis of the tail currents, hyperpolarized after the addition of 8-CPT-cAMP ($V_{1/2}$ changed from 28 to 10.5 mV; Fig. 2 D). Satu-

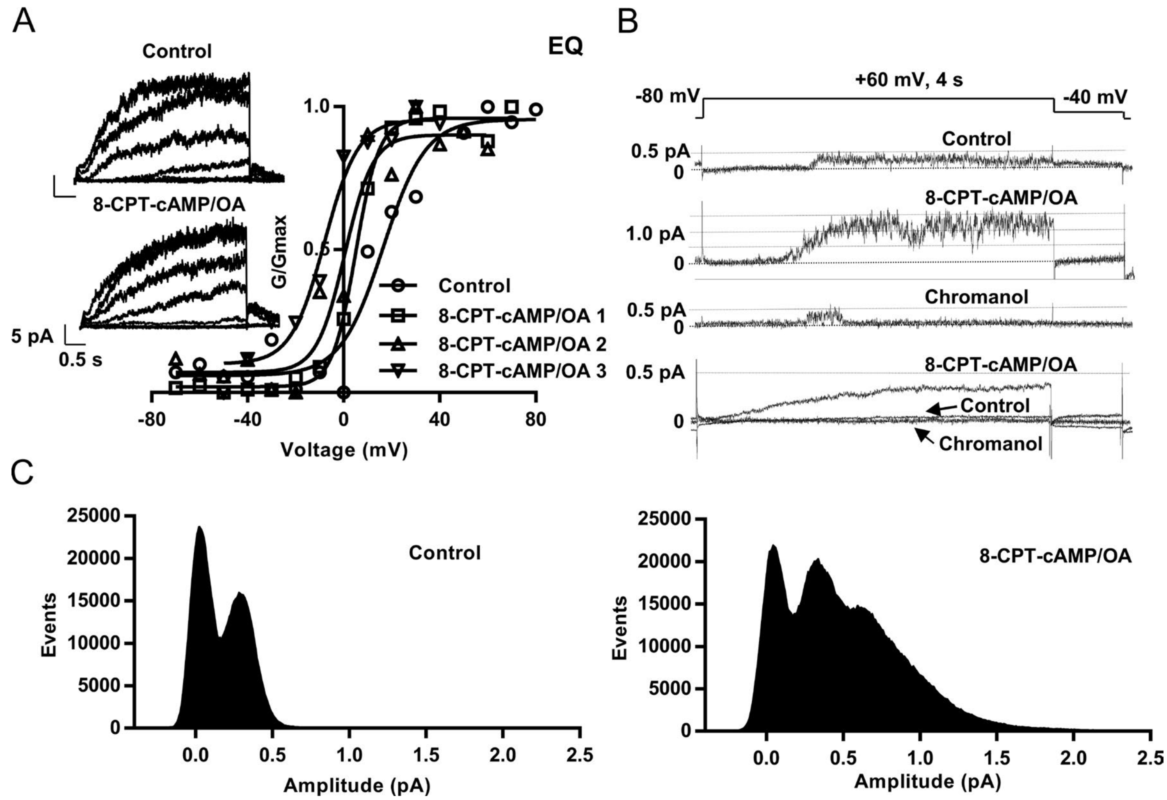

Figure 3. **8-CPT-cAMP hyperpolarizes EQ activation and can increase the number of active channels in cell-attached patches.** (A) G-V curves from a single macropatch before (control, circles, $V_{1/2}$ = 16.4 mV) and after 5-min (squares, #1, $V_{1/2}$ = 5 mV), 8-min (triangles, #2, $V_{1/2}$ = 0.5 mV), and 14-min (upside-down triangles, #3, $V_{1/2}$ = −8 mV) after 200 µM 8-CPT-cAMP/0.2 µM OA exposure. Insets show macropatch I-V currents (control and 8-CPT-cAMP). Cells were held at −60 mV and pulsed from −70 mV to 80 mV in 10-mV steps for 4 s, then to −40 mV for 900 ms. Every other sweep is shown. (B) Sample single-channel sweeps from an I_{Ks}-expressing cell-attached patch in control, after adding 8-CPT-cAMP, and then in 50 µM chromanol 293B. Bottom, ensemble average current before and after 8-CPT-cAMP and after adding chromanol 293B. Control is the mean of 100 sweeps, 8-CPT-cAMP is the mean of 79 sweeps, and chromanol 293B is the mean of 38 sweeps. (C) Raw all-point amplitude histograms of active sweeps in control (left, 21 active sweeps) and when exposed to 8-CPT-cAMP (right, 47 active sweeps).

ration of current activation occurred at less-depolarized voltages in the presence of 8-CPT-cAMP compared with control (Fig. 2 D). This indicates that a major action of 8-CPT-cAMP phosphorylation is to increase the macroscopic channel Po at more negative membrane potentials. These results also show that, at room temperature, we are still able to see the classic effect of 8-CPT-cAMP on the I_{Ks} current.

Response of I_{Ks} to cAMP in cell-attached recordings

In cell-attached recordings, an EQ tandem construct was used to force a 4:4 KCNQ1:KCNE1 I_{Ks} stoichiometry and ensure that the channel complex was fully saturated with E1. This construct has been previously characterized by Murray et al. (2016); in the present experiments, single channels were found to be modulated by 8-CPT-cAMP in the same manner as Q1+E1 expressed separately (Figs. S1 and S2). Cell-attached macropatch recordings were made from multiple channels under the pipette tip. 8-CPT-cAMP addition caused a hyperpolarizing shift in the $V_{1/2}$ of activation for EQ and E1+Q1 (Fig. 3 A and Fig. S2 A), also seen at the whole-cell level with Q1+E1 (Fig. 2 D). This shift increased with longer exposure to 8-CPT-cAMP, with a mean hyperpolarizing shift of −25 ± 8.5 mV in the $V_{1/2}$ of activation (Fig. S3 A). Deactivation appears to also be affected by the addition of 8-CPT-cAMP, as the macropatch tail currents decay more slowly (Fig. 3 A, insets). Of six macropatches for EQ and Q1+E1, two showed an increase in the amplitude of cell-attached macropatch currents.

I_{Ks} single-channel kinetics in the presence of 8-CPT-cAMP

8-CPT-cAMP stimulation affected single-channel properties of I_{Ks} in a number of ways, as illustrated in Figs. 3 and 4. Characteristically, in control, I_{Ks} single-channel currents have a long first latency, and once they appear, channels flicker rapidly in bursts with infrequent longer closings (Figs. 3 B and 4 A). After 200-Hz filtering, single-channel openings peak at less than 0.5 pA with only one active channel present. The all-points histogram of amplitude events from 21 active of 100 sweeps

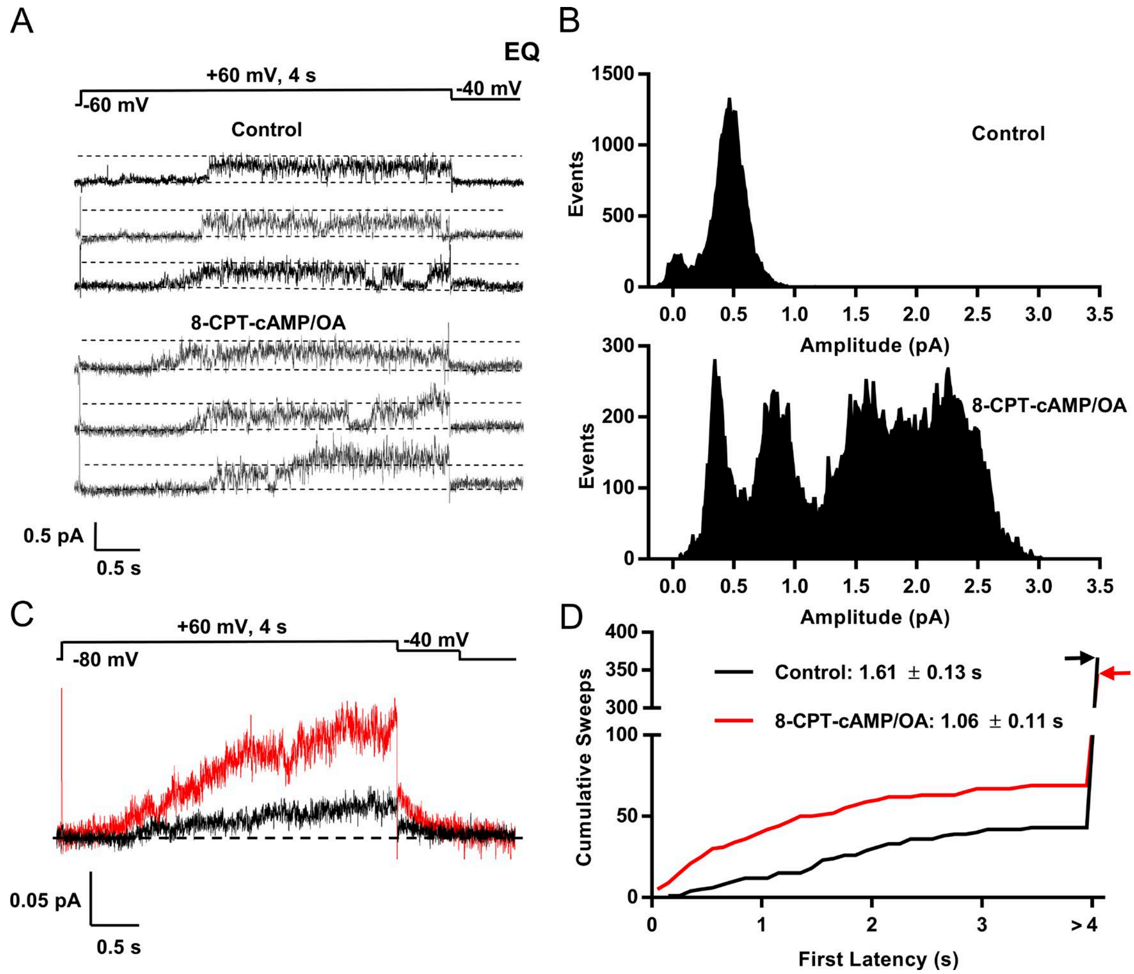

Figure 4. **8-CPT-cAMP increases the ensemble average current and shortens the first latency in EQ.** (A) Single-channel sweeps of EQ coexpressed with Yotiao in control (top) and when exposed to 200 µM 8-CPT-cAMP/0.2 µM OA (bottom). (B) Raw all-points histogram of an example active control sweep (top) and an active sweep during cAMP exposure (bottom). (C) Ensemble average currents from a single patch: 93 sweeps in control, 17 active and 76 blank (black line), and 93 sweeps in 8-CPT-cAMP/OA, 39 active and 54 blank (red line). (D) Cumulative latency histogram. Mean first latency for the 43 active control sweeps of 367 was 1.61 ± 0.13 s. In 200 µM 8-CPT-cAMP/0.2 µM OA, mean first latency for the 69 active sweeps of 367 was 1.06 ± 0.11 s; P = 0.0005 (see Table 1). Sweeps without activity were given a first latency >4 s; arrows indicate sweep total in each case. Note split-scale ordinate.

peaked at 0.38 pA with evidence of only a single channel present despite tens of thousands of opening events (Fig. 3 C, left). Similar results were seen in 100 control sweeps from a second patch (single sweep histogram shown in Fig. 4 B). However, after the administration of 8-CPT-cAMP, an increase in the current amplitude was observed from just under 0.5 pA to 1.5 pA (Fig. 3 B) and up to 2.5 pA in Fig. 4 B (bottom). An additional event peak was seen in the histogram of the 47 active 8-CPT-cAMP sweeps at 0.75 pA, and the range of the histogram included events at 1.5–2.0 pA, suggesting that there were now two to three channels active in the patch (Fig. 3 C, right). Data from the patch shown in Fig. 4 suggest that there were now approximately six channels active after addition of 8-CPT-cAMP (Fig. 4 B, bottom). In the presence of the selective blocker chromanol 293B, this increased current was almost abolished, suggesting that it arose from the presence of more active I_{Ks} channels. In the bottom panel of Fig. 3 B, ensemble averages are shown of the current in all 100 control, 79 8-CPT-cAMP, and 38 chromanol 293B sweeps. The mean current was much greater when 8-CPT-cAMP was present and least when chromanol 293B was added. Overall, in 20 initially single-channel EQ or E1+Q1 patches in control, there was an increase in the apparent number of active channels in nine exposed to 8-CPT-cAMP.

The amplitude of single-channel openings appeared unchanged in the presence of 8-CPT-cAMP. For EQ, the mean single-channel conductance in control was 2.9 pS and unchanged after cAMP. For E1+Q1, the mean single-channel conductance in control was 2.7 pS and 2.8 pS after 8-CPT-cAMP. These values are close to the single-channel conductance of 3.2 pS reported by Werry et al. (2013). Ensemble average (93 sweeps) currents at 60

Table 1. **First latency data of EQ, S209F, S27D, S27D/S92D, and Q1+E1 before and after 200 µM 8-CPT-cAMP/0.2 µM OA**

Construct	Control					8-CPT-cAMP/OA					P-value	Cells
	First latency			Active sweeps	Total sweeps	First latency			Active sweeps	Total sweeps		
	Mean ± SE (s)	95% CI of the mean (lower to upper)	Median (s)	n	n	Mean ± SE (s)	95% CI of the mean (lower to upper)	Median (s)	n	n		n
EQ	1.61 ± 0.13	1.35–1.87	1.57	43	367	1.06 ± 0.11	0.84–1.27	0.85	69	345	0.0005	3
S209F+E1	0.16 ± 0.05	0.07–0.25	0.07	67	128	0.18 ± 0.06	0.06–0.30	0.04	85	220	0.0208	2
S27D+E1	1.81 ± 0.13	1.55–2.08	1.60	57	302	1.44 ± 0.11	1.22–1.66	1.10	67	335	0.0320	3
Q1+E1	1.32 ± 0.13	1.06–1.57	0.90	68	278	0.79 ± 0.08	0.63–0.95	0.50	104	309	0.0002	3
S27D/S92D+E1	1.62 ± 0.08	1.46–1.78	1.40	189	467	1.43 ± 0.13	1.18–1.69	1.26	60	119	0.332	3–5

Latencies were obtained from 4-s sweeps at 60 mV, active sweeps only. P-values indicate difference between control and cAMP (Mann–Whitney test).

mV from a single-channel patch before and after cAMP are shown in Fig. 4 C. There is an increase in peak ensemble current from 0.04 to 0.12 pA in the presence of 8-CPT-cAMP, which corresponds to an increase in Po from 0.12 to 0.27 in this patch, and agrees quite well with the ~2.5-fold increase in whole-cell current at 60 mV shown in Fig. 2 C.

A consistent increase in the number of active sweeps occurred in the presence of 8-CPT-cAMP and is clearly seen in the latency histogram (Fig. 4 D). In control, 43 of 367 sweeps were active (black line), whereas in 8-CPT-cAMP, 69 sweeps of 345 were active (red line). The mean first latency of EQ I_{Ks} channels was measured from patches in which only a single channel was found to be present, even after exposure to 8-CPT-cAMP, and was 1.61 ± 0.13 s in control. It was significantly shortened upon 8-CPT-cAMP addition to 1.06 ± 0.11 s (Fig. 4 D and Table 1; P = 0.0005, n = 3). These numbers correlate well with the first latency of E1 and Q1 expressed separately (Fig. S1 C; and Table 1) and favorably with changes in the activation time course of EQ macropatches. The time to half-activation at 60 mV was reduced from 1.04 to 0.65 s (n = 4) with 8-CPT-cAMP, a 37% reduction, compared with the 34.2% decrease in first latency for EQ after 8-CPT-cAMP addition (Table 1).

Changes in substate occupancy in the presence of 8-CPT-cAMP are primarily VSD activation effects

In patches with no increase in the number of active channels, we analyzed the occupancy of the subconductance levels of the single channel present in control and after 8-CPT-cAMP addition. During the idealization process (Materials and methods and Fig. S8), we assumed that 8-CPT-cAMP did not change the subconductance amplitude levels reached in control, just the occupancy of these levels. The computer-defined event amplitudes usually clustered closely around these preset levels. The results of this analysis on sweeps from two different EQ patches are shown in Fig. 5, 26 active sweeps before, and 25 sweeps after the addition of 8-CPT-cAMP. The results illustrate the occupancy of five defined EQ I_{Ks} substate levels (0.145–0.75 pA). In Fig. 5 A, the raw all-points histograms for control (blue) and 8-CPT-cAMP (red) are overlaid. The initial peak, or level 0, is the closed state (0 pA). It can already be clearly seen that the area of the envelope to the right of the 0 pA peak, corresponding to channel openings, is greater after exposure to 8-CPT-cAMP (red) than control (blue).

The idealized histograms of the subconductance analysis for control (blue) and 8-CPT-cAMP (red) show the grouping of opening events into the five subconductance levels (Fig. 5 B). We have already established that the 0.29- and 0.44-pA sublevels when data are filtered at 0.2 kHz are the most frequently occupied upper open levels (Werry et al., 2013). The present data were filtered at 0.5 kHz, and in Fig. 5 (B and C), the 0.33- and 0.5-pA levels are the most frequently visited upper open levels, accounting for 2.6% and 3.1% of the total dwell time, respectively. In the presence of 8-CPT-cAMP, there is a clear shift of occupancy away from the closed state to the higher subconductance opening levels. For example, 2.6% of events occurred at the 0.33-pA sublevel in control, but after 8-CPT-cAMP addition, this almost doubled to 4.5%. The 0.5-pA level also saw an increase in the number and doubling in the proportion of events from 3.1 to 7.6%, and the 0.75-pA sublevel increased from 0.8 to 1.7%. The first latencies to opening of each of the six sublevels before and after 8-CPT-cAMP also showed a trend to shorter times to reach each of the levels in the presence of 8-CPT-cAMP, although it was not statistically significant. Similar results were seen in two other EQ or Q1+E1 patches, indicating that phosphorylation of I_{Ks} leads to more frequent high-subconductance-state occupancy, consistent with the increased current levels observed at the microscopic and macroscopic levels.

An analysis of EQ burst kinetics in controls and in the presence of 8-CPT-cAMP is shown in Fig. 6. Bursts of channel openings such as those shown in Fig. 4 and Fig. S1 are largely outside the VSD-driven activation

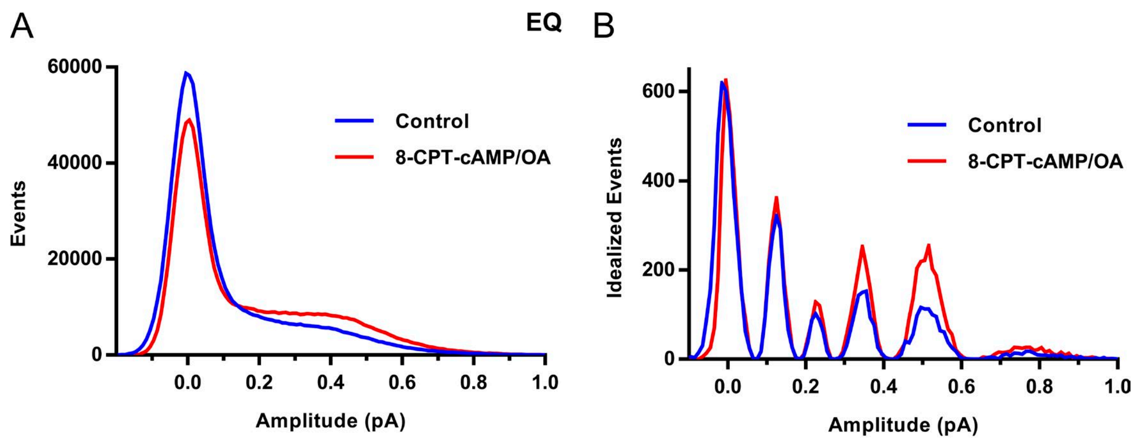

C

Control	Closed	0.145 pA	0.22 pA	0.33 pA	0.5 pA	0.75 pA	All
Total dwell time (ms)	63585.3	3420.4	829.6	1887.2	2243.2	561.2	72527.0
Mean dwell time (ms)	17.13	2.35	2.05	2.16	2.24	2.42	
% of total dwell time	87.7	4.7	1.1	2.6	3.1	0.8	
Number of events	3712	1454	404	873	1000	232	7675

8-CPT-cAMP/OA	Closed	0.145 pA	0.22 pA	0.33 pA	0.5 pA	0.75 pA	All
Total dwell time (ms)	49200.5	3663.6	1034.4	2787.3	4717.3	1048.2	62451.3
Mean dwell time (ms)	16.95	2.31	2.06	2.16	2.37	2.48	
% of total dwell time	78.8	5.9	1.7	4.5	7.6	1.7	
Number of events	2903	1586	503	1292	1992	423	8699

Figure 5. **Subconductance analysis of EQ before and after 8-CPT-cAMP/OA.** (A) Raw all-points amplitude histogram of 26 active control sweeps (blue) and 25 active sweeps after 200 µM 8-CPT-cAMP/OA from two different EQ single patches. (B) Five initial thresholds were used for the idealization: 0.145, 0.22, 0.33, 0.5, and 0.75 pA. For the control histogram, the final idealized levels were 0.14 ± 0.05, 0.24 ± 0.06, 0.34 ± 0.07, 0.51 ± 0.08, and 0.74 ± 0.10. In the presence of 8-CPT-cAMP/OA, the final idealized levels for cAMP were 0.13 ± 0.05, 0.23 ± 0.05, 0.34 ± 0.06, 0.49 ± 0.07, and 0.70 ± 0.08. (C) Total and mean dwell times (milliseconds) for each of the different thresholds, the percentage of time spent at each level, and number of events at each threshold before and after 8-CPT-cAMP. The data were filtered at 0.5 kHz, and the bin width used was 0.01 pA. Only events longer than 1.5 ms were included.

pathway (Werry et al., 2013) and allow us to examine the effects of 8-CPT-cAMP on pore kinetics of EQ. After idealization of 26 control and 25 8-CPT-cAMP 4-s sweeps, we found two resolvable closed states for EQ with similar time constants to those we reported previously in Werry et al. (2013). In the presence of cAMP, there is no change in the mean closed time for the vast majority of events. For the longer closed time, there was an increase, but there are few events for this fit (Fig. 6 A). Interestingly, the closed dwell times of EQ in 8-CPT-cAMP are very close to those reported for S209F + E1 in Eldstrom et al. (2015). A probability plot of the closed dwell time distribution shows clearly how the burst closing kinetics are unaffected by 8-CPT-cAMP (Fig. 6 B). Peaks of the closed dwell time distribution at ~2 and 10 ms are very similar in both control and 8-CPT-cAMP.

The table in Fig. 5 C shows a measure of the mean dwell times at each sublevel; they were relatively unchanged in the presence of 8-CPT-cAMP, with some dwell times increasing and some decreasing. The data give an indication of the time the channel spent bursting at a particular sublevel before moving to a higher or lower subconductance level. A more formal analysis of overall open burst durations was performed using a burst termination criterion of pore closing for >2 ms. The event histograms were fitted as the sum of two decay exponentials, the faster of which accounted for >90% of bursts and had time constants of 2.9 ± 0.07 ms in control and 2.5 ± 0.09 ms in 8-CPT-cAMP. The burst duration probability functions are shown together in Fig. 6 C and appear unaffected by cAMP addition (Fig. 6 C). In fact, there is a small but significant decrease in the number of bursts at intermediate dwell times in the presence of 8-CPT-CAMP. Overall, these data suggest that 8-CPT-cAMP has only minor effects, both positive and negative, on channel pore kinetics.

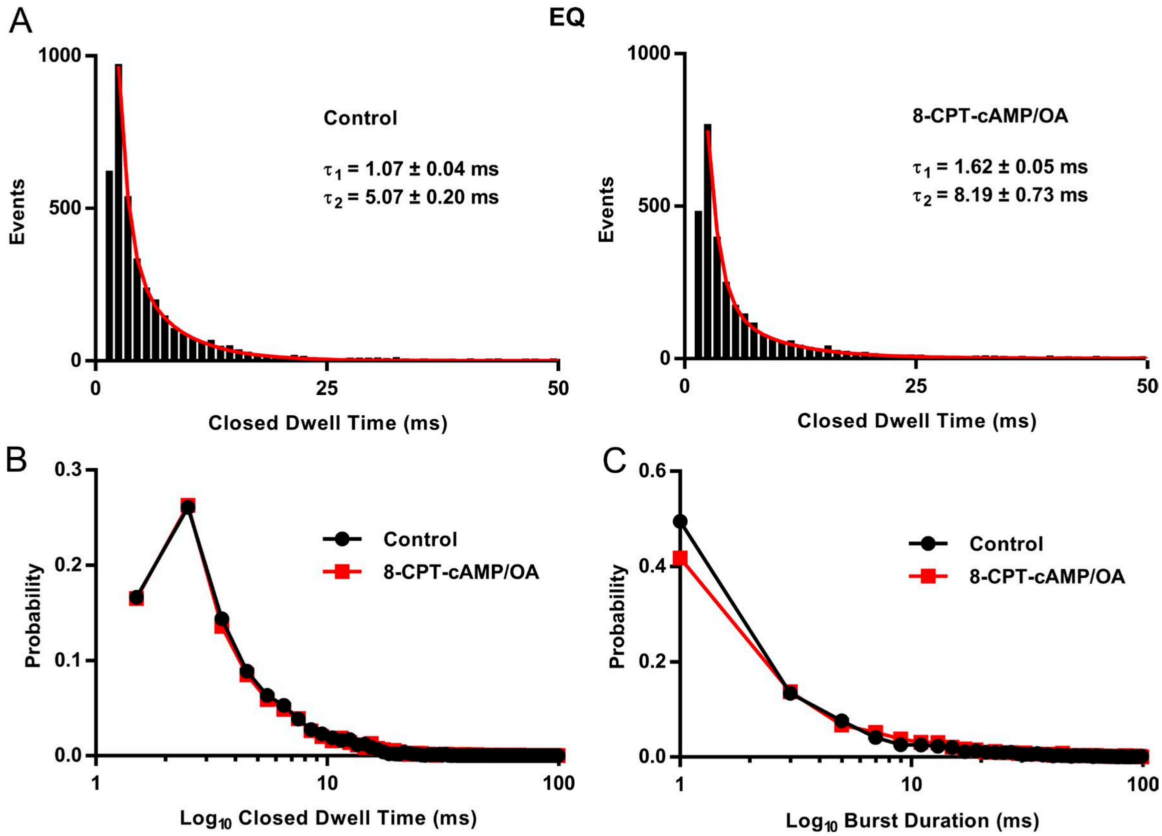

Figure 6. **EQ closed dwell times and burst analysis.** (A) Closed dwell time distributions for EQ from 26 sweeps before and 25 sweeps after 200 µM 8-CPT-cAMP/0.2 µM OA, filtered at 500 Hz. Data were fitted with the sum of two exponential functions. τ_1: 1.07 ± 0.04 ms (]area under the curve [AUC 606.85 ± 19.05) and τ_2: 5.07 ± 0.20 ms (AUC 359.10 ± 18.75) in control. After 8-CPT-cAMP/OA, τ_1: 1.62 ± 0.05 ms (AUC 613.43 ± 14.06) and τ_2: 8.19 ± 0.73 ms (AUC 117.49 ± 14.00). Bin width was 1 ms. (B) Probability distribution of closed time durations in control (black) and after 8-CPT-cAMP/OA (red), from data in A. (C) Probability distribution of burst durations in control (black) and after 8-CPT-cAMP/OA (red), from the data used in A. Event histograms were fitted with the sum of two exponential functions. In control τ_1: 1.58 ± 0.05 ms (AUC 1662.64) and τ_2: 17.26 ± 2.56 ms (AUC 136.94 ± 17.69). In 8-CPT-cAMP, τ_1: 1.99 ± 0.06 ms (AUC 1073.46 ± 15.72) and τ_2: 22.36 ± 3.31 ms (AUC 95.62 ± 12.35). Bin width was 2 ms. Only events longer than 1.5 ms in duration were used in this analysis.

8-CPT-cAMP effects on I_{Ks} mutants described as having fixed and activated VSDs

E160R/R237E (E1R/R4E) KCNQ1, a charge reversal mutant suggested to lock the voltage sensors in an upward position and stabilize the position of the VSD (Wu et al., 2010; Zaydman et al., 2014), was used to further test the action of 8-CPT-cAMP by isolating VSD-induced changes in the channel complex and allowing a direct test on pore kinetics. In controls, when E1R/R4E is coexpressed with KCNE1 (Fig. 7, A–C, left), at 40 mV channels opened without any latency and burst throughout 4-s sweeps, as well as during repolarization to −40 and −80 mV. The ensemble average current (Fig. 7 A, middle) was time-independent compared with WT I_{Ks} (Fig. 3 B) and unaffected by 8-CPT-cAMP, but still sensitive to chromanol 293B (Fig. 7 A, bottom).

All-points histograms reveal a distribution of openings with the major event peak at ~0.35 pA at this potential. The mean single channel conductance was 3.2 pS and was unchanged in the presence of 8-CPT-cAMP (n = 5). These values may be compared with a conductance of 2.9 pS in EQ channels before and after exposure to cAMP (see Fig. 4 legend). The histograms show that the effect of cAMP in the same single-channel patch was to decrease the closed-state occupancy without significantly changing numbers of events at the higher-subconductance-occupancy levels shown in Fig. 7 C at ~0.55 pA. As a result, there was little effect on the ensemble current (Fig. 7 A, middle). These changes are in contrast to the shortened latency to opening and occupancy of higher sublevels seen in EQ channels (Figs. 4 and 5) and increased EQ and E1+Q1 ensemble currents (Fig. 4 C and Fig. S2 B) during exposure to 8-CPT-cAMP. Similar results have been observed in four other E1R/R4E patches.

KCNQ1 S209F is a gain-of-function mutation found in the S3 domain of the VSD (Eldstrom et al., 2010) and is like E1R/R4E in that it has a saturated Po over a wide potential range. S209F+E1 has been previously characterized as having a much higher open probabil-

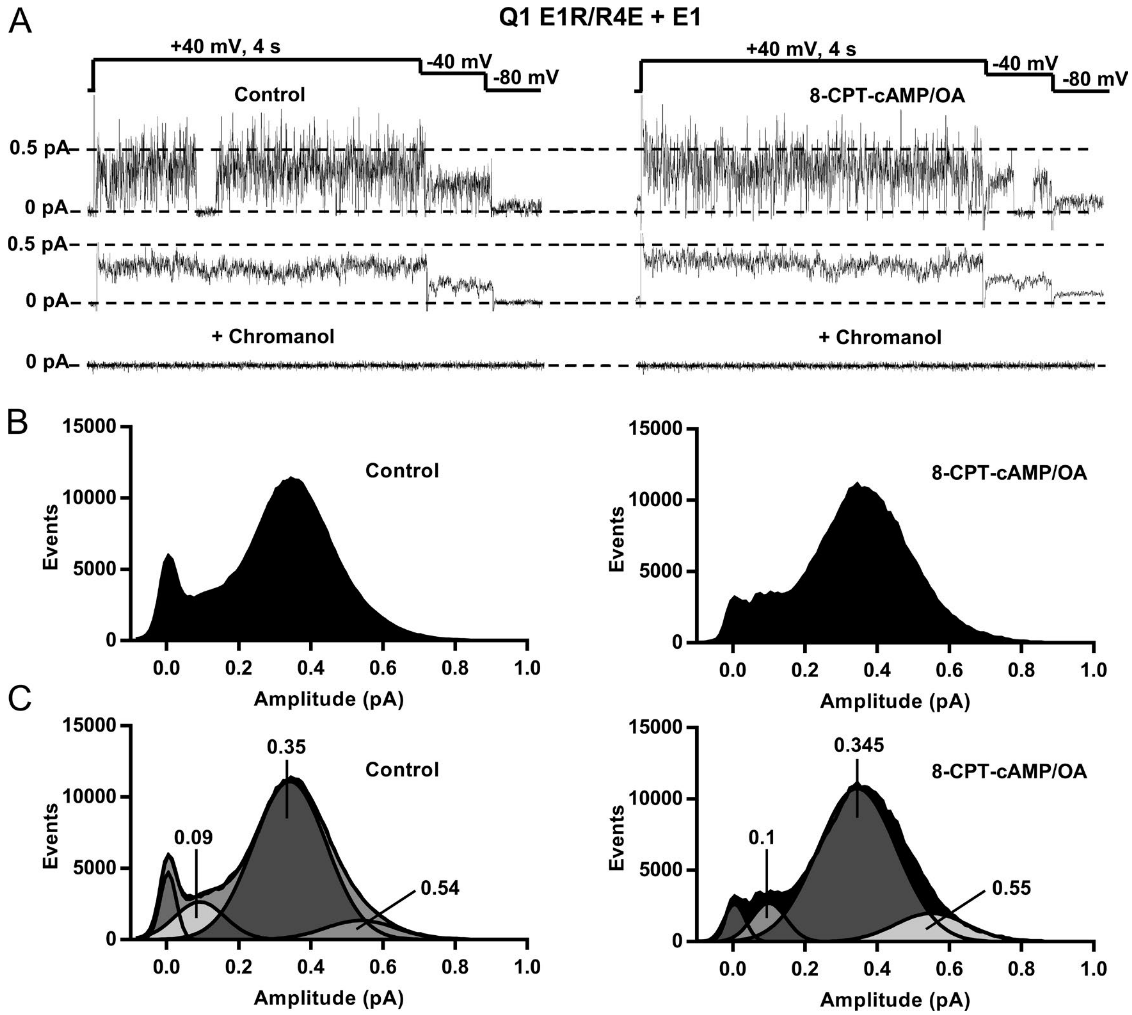

Figure 7. **The mutant E1R/R4E + E1 channel is unaffected by 8-CPT-cAMP.** (A) Top, single-channel sweep of Q1 E1R/R4E+E1 expressed with Yotiao before and after 200 µM 8-CPT-cAMP/0.2 µM OA. Middle, ensemble averages of 10 sweeps pulsed to 40 mV before and after 8-CPT-cAMP. Bottom, mean currents after addition of 50 µM chromanol 293B. (B) All-points histograms from 10 sweeps before and after 8-CPT-cAMP. (C) Gaussian fits of the histograms shown in B and the amplitudes of individual fitted peaks as determined with Clampfit.

ity than that of WT I_{Ks}, (Po = 0.6 compared with 0.15 in WT after 4 s at 60 mV; Werry et al., 2013; Eldstrom et al., 2015), with dominant residency in higher subconducting open states. At room temperature, whole-cell experiments on S209F revealed that it possesses almost voltage-independent gating when expressed with E1 (Fig. S6 A). Currents are fairly time independent, and the Po shows only a small decrease negative to −50 mV (Fig. S6 B). No effect of 8-CPT-cAMP on G-V relationships or current amplitude was seen at the whole-cell level (Fig. S6, B and C).

Because this mutant already has activated and equilibrated VSD gating, it can provide a good test of cAMP on pore kinetics at positive potentials. Data in Fig. 8 A show single sweeps of S209F+E1 at 60 mV. From these representative traces, it can be seen that the channel opens with little latency but still sometimes occupies lower sublevels before reaching higher subconductance states. The single-channel currents for S209F before and after 8-CPT-cAMP appear to be very similar and show that the time the channel is open is greatly increased compared with that of EQ (Figs. 3 B and 4 A), but perhaps less than E1R/R4E, as judged by the relative number of closed events in the all-points histograms (Fig. 8 B).

The active peaks of the raw histograms higher than 0.4 pA enclose a much larger number of events than the closed events peak (compare with EQ or WT Q1+E1; Fig. 3 C and Fig. S1 B). There is not much difference in the numbers of closed events before and after cAMP, but there is a shift of open events from lower to higher open subconductance levels in S209F in the presence of cAMP and an increase in the amplitude corresponding to the event peak of the histogram. Before addition of 8-CPT-cAMP, the event peak amplitude was 0.38 pA, and after, 0.42

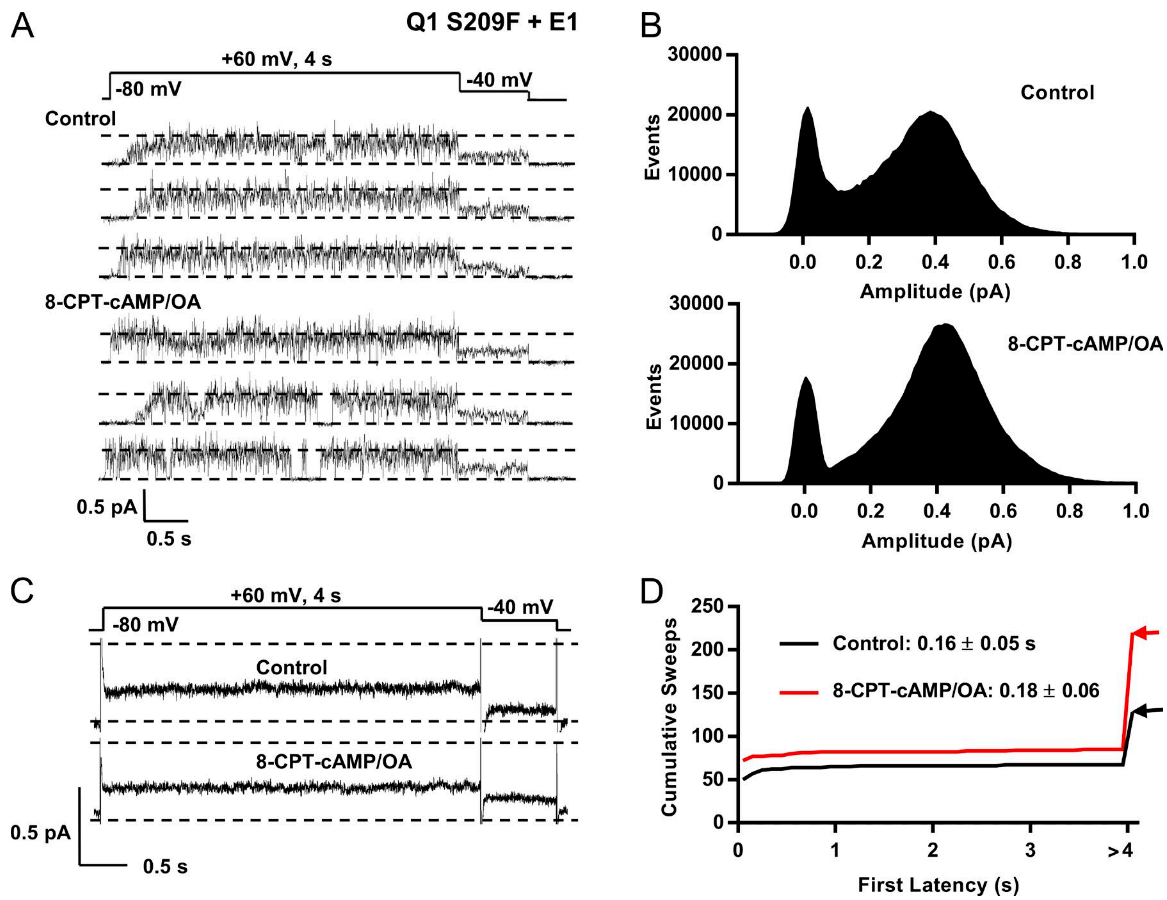

Figure 8. **8-CPT-cAMP has a small kinetic effect on the high Po mutant Q1 S209F coexpressed with E1.** (A) S209F+E1 and Yotiao. Representative single channel sweeps are shown in control (top) and during exposure to 200 µM 8-CPT-cAMP/0.2 µM OA (bottom). (B) All-points amplitude histograms in control (top, 21 active sweeps) and during 8-CPT-cAMP exposure (bottom, 27 active sweeps). (C) Ensemble average currents from a single patch; 70 control sweeps (50 active and 20 blank) and 70 sweeps in 8-CPT-cAMP/OA (55 active and 15 blank). Control and 8-CPT-cAMP/OA averages peaked at 0.25 pA after 4 s at 60 mV. (D) Cumulative latency histogram. Mean first latency for the 67 active control sweeps of 128 was 0.16 ± 0.05 s. With 200 µM 8-CPT-cAMP/0.2 µM OA, mean first latency for the 85 active sweeps of 220 was 0.18 ± 0.06 s; P = 0.021 (see Table 1). Sweeps without activity were given a first latency >4 s.

pA (Fig. 8 B). As in whole-cell data, there was no change in ensemble average single-channel currents at 60 mV (Fig. 8 C) and 0 mV (not depicted) after exposure to 8-CPT-cAMP, with a calculated Po of 0.71 at 60 mV (control) and 0.74 (8-CPT-cAMP; Fig. 8 C). S209F first latency was markedly reduced compared with that of WT Q1+E1. In S209F patches in control, first latency was 0.16 ± 0.05 s, and upon 8-CPT-cAMP addition, actually lengthened to 0.18 ± 0.056 s, although the median value declined (Fig. 8 D; and Table 1). There was also no increase in the number of active sweeps and no recruitment of new or silent channels upon 8-CPT-cAMP administration, such as that seen with EQ or WT Q1+E1 (Figs. 3 B and 4 B and Fig. S2 C).

Both E1R/R4E and S209F are mutations described as having fixed and activated VSDs, and our data indicate that their overall gating is relatively unaffected by 8-CPT-cAMP, which suggests that the actions of 8-CPT-cAMP on the channel complex are mediated principally via the voltage sensor domains.

Effect of 8-CPT-cAMP on the pseudo-phosphorylated I_{Ks} channel mutants S27D and S27D-S92D

The Ser[27] residue in Q1 is a phosphorylation site known to be important in the response of I_{Ks} to β-AR stimulation (Fig. 1; Kurokawa et al., 2003), and S27D is a phosphomimetic mutant that recapitulates most of the effects seen with phosphorylation of I_{Ks}. However, the S27D+E1 macropatch data still showed a hyperpolarizing shift in the $V_{1/2}$ of activation after 8-CPT-cAMP addition, as shown in Fig. 9 A (−15.4 mV). The mean hyperpolarization in S27D macropatches in the presence of 8-CPT-cAMP was from 13.1 to −1.1 mV (−14.3 mV, $n = 3$; Fig. S3 B), compared with a hyperpolarization from 27.0 to 2.1 mV (−24.9 mV) for EQ ($n = 4$; Fig. S3 A). Deactivation also appeared to be slowed when 8-CPT-cAMP was added (Fig. 9 A, insets). The single-channel recordings are

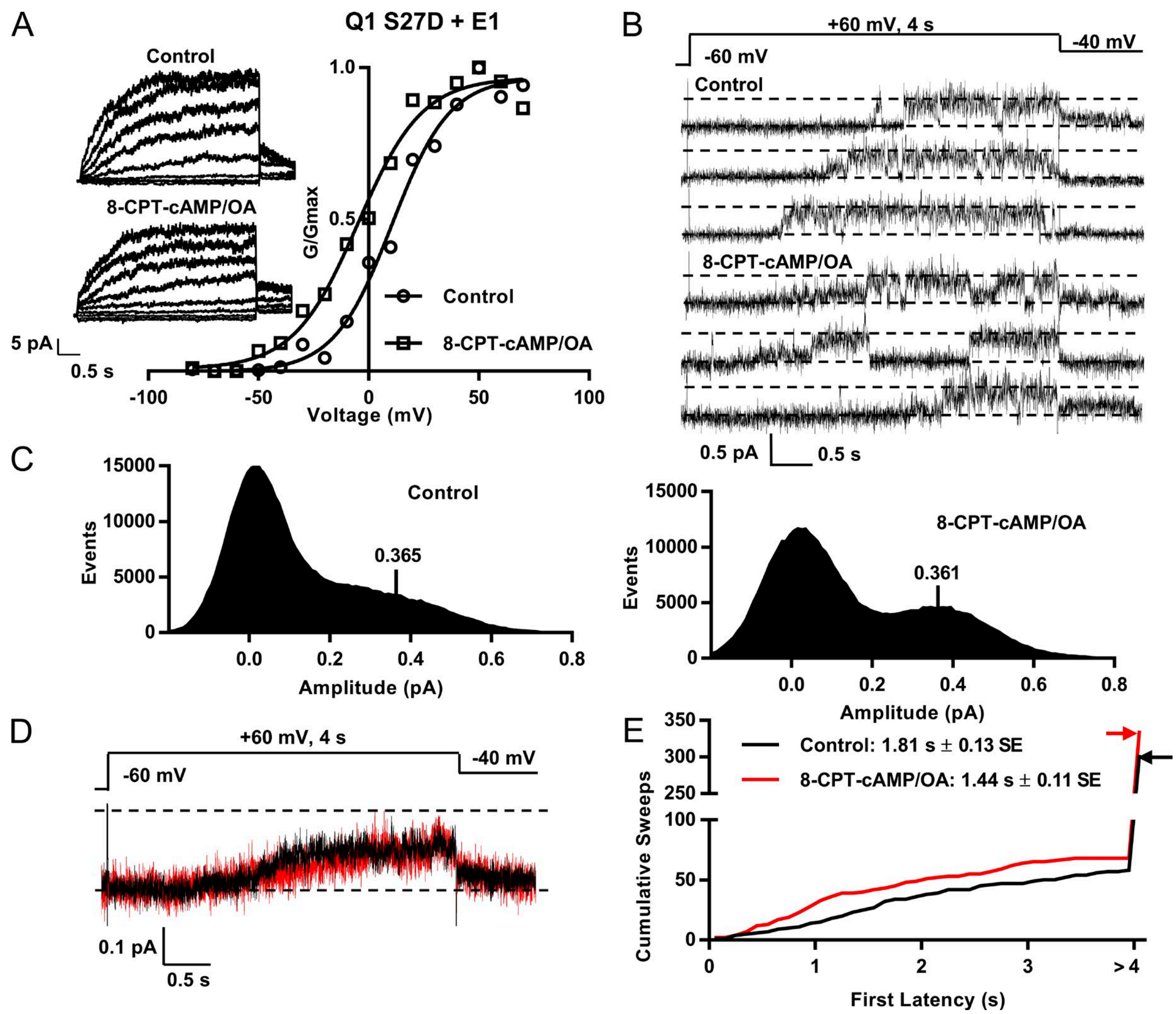

Figure 9. **Effects of 8-CPT-cAMP on first latency of Q1 S27D+E1 and Yotiao.** (A) G-V curves from macropatches in control and after exposure to 200 µM 8-CPT-cAMP/0.2 µM OA. Graph shows mean of *n* = 2 in each case from a single macropatch in control (circles, $V_{1/2}$ = 10.5 mV) and cAMP (squares, $V_{1/2}$ = −4.9 mV). Insets show macropatch I-V currents in control and with 8-CPT-cAMP. Every other sweep is shown. Cells were held at −60 mV then pulsed from −80 mV to 80 mV in 10-mV steps for 4 s. They were then pulsed to −40 mV for 900 ms. (B) Single-channel sweeps of Q1 S27D+E1 and Yotiao in control (top) and exposed to cAMP (bottom). (C) All-point amplitude histograms of active control sweeps (left, 11 sweeps) and active sweeps during cAMP exposure (right, 11 sweeps) were fitted with event peaks in control of 0.37 pA and in 8-CPT-cAMP of 0.36 pA. (D) Ensemble average currents from a single patch; 31 control sweeps (14 active) and 31 sweeps in 8-CPT-cAMP/OA (15 active). Control and 8-CPT-cAMP/OA averages peaked at 0.12 pA after 4 s at 60 mV. (E) Cumulative latency histogram. Mean first latency for the 57 active control sweeps of 302 was 1.81 ± 0.13 s. With 200 µM 8-CPT-cAMP/0.2 µM OA, mean first latency for the 67 active sweeps of 335 was 1.44 ± 0.1 s; P = 0.032 (see Table 1). Sweeps without activity were given a first latency >4 s. Note split-scale ordinate. Bin width of the histogram was 0.01 pA.

shown in Fig. 9 B, and there were more subtle changes in the kinetics with 8-CPT-cAMP than seen in EQ channels. The all-points histograms showed a relative reduction of closed-state occupancy and a small shift of open events to higher subconductance amplitudes (Fig. 9 C). The amplitude of the single-channel events peak was unchanged though, as all-point histograms of 11 active control and 11 active 8-CPT-cAMP sweeps were fitted with an event peak at 0.365 pA in control and 0.361 pA with 8-CPT-cAMP/OA (Fig. 9 C). As might be expected from the all-points histograms, there was little change in ensemble average currents at 60 mV (Fig. 9 D) in S27D after exposure to 8-CPT-cAMP, with a calculated Po of ~0.33 in control and 8-CPT-cAMP.

The detailed changes in subconductance occupancy were analyzed after data idealization, and results are shown in Figs. S4 and S5. It is of note that the closed dwell time in S27D as a proportion of the total in control (78%) is very similar to that seen in EQ after exposure to 8-CPT-cAMP (78.8%; Fig. 5 C). However, there is a reduction of closed-state occupancy and a shift of subconductance occupancy to all the higher sublevels after cAMP/OA exposure. The first latency was also still significantly shortened by the addition of 8-CPT-cAMP

(Fig. 9 E), from 1.81 ± 0.13 to 1.44 ± 0.11 s (Table 1; P = 0.032), and overall, these changes after cAMP are very similar to those seen in EQ and E1+Q1 channels but are attenuated as expected in this mutant. There were few changes in the burst kinetics in the S27D mutant after exposure to 8-CPT-cAMP (Fig. S5).

Ser^{92} is also a potential phosphorylation site in the N terminus of KCNQ1 (Lopes et al., 2007) that has been shown to increase I_{Ks} current (Lundby et al., 2013), and thus we were prompted to test the effects of 8-CPT-cAMP/OA on the double-mutant S27D/S92D-Q1 channel (Fig. 10). Surprisingly, the G-V relationship was slightly depolarized from the WT I_{Ks} relationship, rather than hyperpolarized, but there was no further change upon exposure to 8-CPT-cAMP. There was no change in peak whole-cell currents with cAMP, and no change in single-channel peak event amplitudes or latency kinetics, although we did not perform a subconductance analysis (Fig. 10, C and D). The mean first latency in control was 1.62 ± 0.08 s and was not significantly different in the presence of 8-CPT-cAMP, at 1.43 ± 0.13 s (Table 1; P = 0.332). These results suggest that almost all of the kinetic effects of 8-CPT-CAMP on I_{Ks} channels are mediated via phosphorylation of these two residues, Ser^{27} and Ser^{92}.

Effect of 8-CPT-cAMP on the surface expression of WT I_{Ks}

To investigate whether the recruitment of WT I_{Ks} channels in the single-channel patches and whether an increased current density at the whole-cell level could be in part because of an increase in channels present at the cell surface, total internal reflection fluorescence (TIRF) microscopy was used to allow visualization of channels within 80 nm of the surface of the cell and monitor channel trafficking (Schwarzer et al., 2013; Yamamura et al., 2015).

CHO cells transfected with WT KCNQ1-GFP and WT KCNE1-mCherry were recorded for a period of 15–30 min, and 200 µM 8-CPT-cAMP was added at 5 min. TIRF images of KCNQ1-GFP and KCNE1-mCherry at 0 and 15 min, respectively, are shown in Fig. 11 (A and C); 8-CPT-cAMP was added at 5 min. After measuring the fluorescence intensity of the whole cell, there does not appear to be an increase in the overall surface expression of KCNQ1-GFP or KCNE1-mCherry after the addition of 8-CPT-cAMP (Fig. 11, B and D). This indicates that addition of cAMP does not increase the net trafficking of I_{Ks} to the cell surface.

It was clear from observation of the KCNQ1-GFP fluorescence signals over the time frame of 15–30 min that the channels are highly mobile in both the presence and absence of 200 µM 8-CPT-cAMP (Fig. S7 A). Some ROIs did show a decrease or an increase (Figs. S7, A and B) in fluorescence intensity with cAMP exposure, indicating that channels had internalized or been inserted at these locations during the experiment. In Fig. S7 A, a cell with three chosen ROIs is shown before (0 or 15 min) and after (30 min) addition of 8-CPT-cAMP. ROI 1 shows a decline in fluorescence intensity immediately after addition of 8-CPT-cAMP (Fig. S7 B, left). Before addition of 8-CPT-cAMP, the fluorescence at 15 min was 385 a.u.; after addition of 8-CPT-cAMP, at 30 min, it had dropped to 354 a.u. (Fig. S7 B, left). In ROI 2, the number of KCNQ1-GFP channels increased shortly after 8-CPT-cAMP was added (Fig. S7 B, middle). The fluorescence intensity went from a stable baseline at 215 a.u. to 230 a.u. (Fig. S7 B, middle). Finally, the largest increase is seen in ROI 3, in which the fluorescence intensity increases from 270 to 350 a.u. after addition of 8-CPT-cAMP (Fig. S7 B, right). However, when analysis was expanded to 54–61 ROIs from the border region of the cell and 52–64 ROIs from the cell center of 11 cells before and after 2-, 5-, and 10-min exposure to 8-CPT-cAMP (Fig. S7 C), the mean fluorescence intensities of ROIs did not change significantly from those in the center to those in the border over the 10 min analyzed, in control conditions (Fig. S7 C, left) or during exposure to 8-CPT-cAMP (Fig. S7 C, right). This supports the conclusion that addition of cAMP does not lead to any organized redistribution of the channel or increase in net trafficking to the surface.

DISCUSSION

The mechanism behind the increase in I_{Ks} current after cAMP administration has not been fully defined. It is well understood at the whole-cell level that there is a hyperpolarization of the G-V relationship and that there must be effects on the channel complex Po, but these have not been studied before at the single-channel level. The underlying mechanisms for the cAMP-induced increase in current were an increased likelihood of channels to open at all during 4-s depolarizations, the ability of the channels to open sooner during a depolarizing test pulse than in control, and to occupy higher subconducting states more frequently. The studies with the E1R/R4E and S209F KCNQ1 mutants indicated that these dominant effects of cAMP were mediated preferentially via effects on voltage sensor domain kinetics rather than changes in pore kinetics. Our experiments also revealed that the effects of 8-CPT-cAMP on I_{Ks} single-channel kinetics could largely be mimicked by Asp substitution at Ser^{27} and Ser^{92}.

We have proposed that there may be an increase in the number of I_{Ks} channels at the cell surface that could increase overall current. Indeed, in cell-attached single-channel and macropatch recordings, we could often see an increase in the number of active channels after the addition of the cAMP analog. However, our TIRF results showed that there is no net increase in the number of channels present and ac-

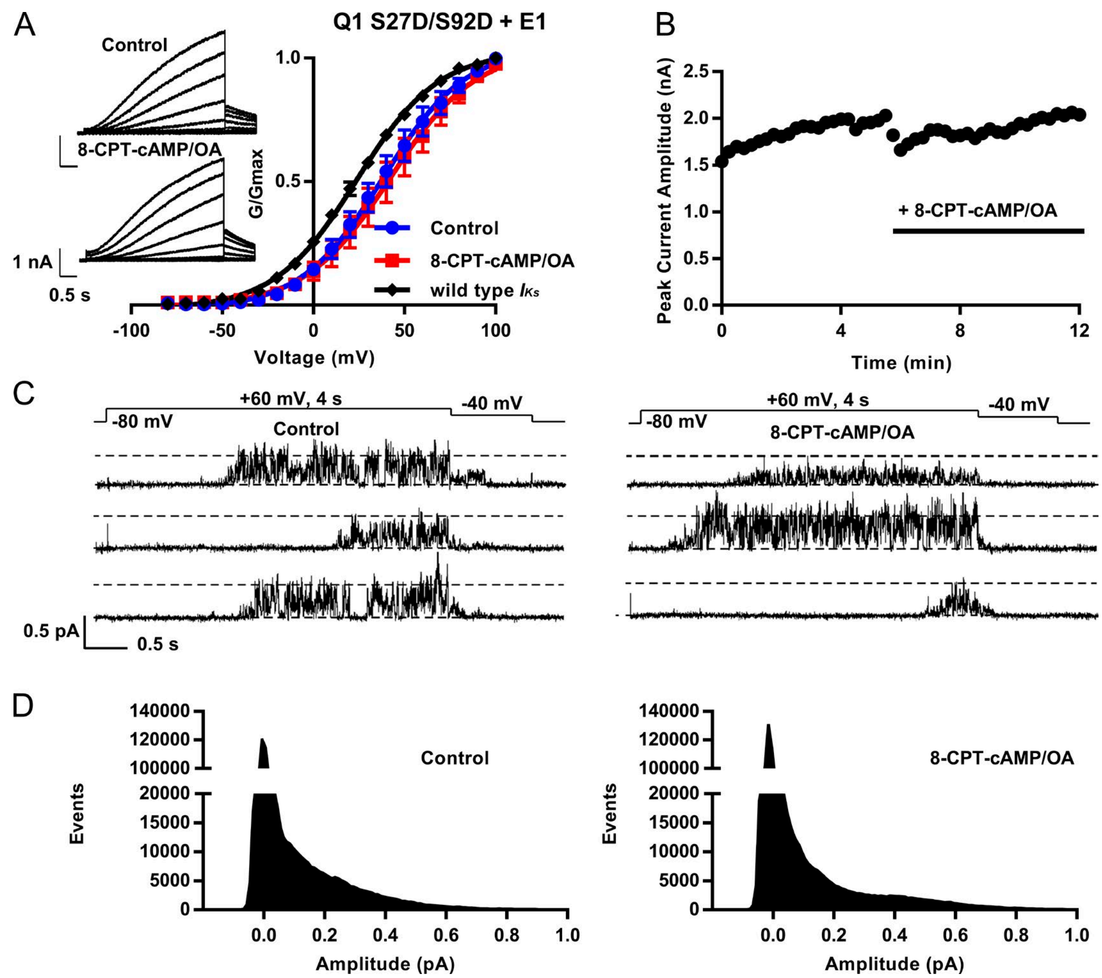

Figure 10. **Effects of 8-CPT-cAMP on currents in Q1 S27D/S92D+E1 and Yotiao.** (A) G-V curves from whole-cell measurements in control ($V_{1/2}$ = 43 ± 6.9 mV) and after exposure to 200 µM 8-CPT-cAMP/0.2 µM OA ($V_{1/2}$ = 47.5 ± 8.6 mV, n = 8 cells), compared with WT I_{Ks} ($V_{1/2}$ = 25.1 ± 2.5 mV). Error bars show ±SE. Insets show I-V currents in control and with 8-CPT-cAMP. Every other sweep is shown. Cells were held at −90 mV and pulsed from −80 mV to 100 mV in 10-mV steps for 4 s. Tail currents were recorded at −40 mV for 900 ms. (B) Diary plot of the peak outward current during a 4-s pulse to 60 mV over time. Bar indicates the addition of 200 µM 8-CPT-cAMP/0.2 µM OA to the bath. (C) Sample single-channel sweeps of S27D/S92D+E1 before (left) and after (right panel) 8-CPT-cAMP. (D) Raw all-point amplitude histograms of 21 active S27D/S92D sweeps before (left) and after (right) 8-CPT-cAMP/OA.

tive on the surface of cells, and although the data do support a constant redistribution of channels across the cell surface, this was not significantly changed by cAMP administration.

Single channel studies of I_{Ks}

The fusion construct EQ is composed of one E1 and one Q1 subunit attached together by a linker as characterized in (Murray et al., 2016). The response to 8-CPT-cAMP was tested on independently expressed Q1 and E1 subunits, and they responded similarly to the tandem EQ construct (Figs. S1 and S2). Half the time, both constructs also showed an increase in the number of channels in the patch after cAMP addition. Single-channel recordings of both EQ and Q1+E1 show the characteristic long latencies to the initial opening of the channel, and their properties are similar to those previously reported for these constructs when AKAP-9 was not transfected (Murray et al., 2016). However, once the cAMP analog was added, this first latency was significantly decreased (Fig. 4 D; and Table 1) and the channel opened more quickly upon depolarization (Fig. 2 C). The number of active sweeps also increased by ~70% upon 8-CPT-cAMP stimulation (Fig. 4 D).

I_{Ks} has a number of discernible subconducting levels (Fig. S8) that are transitioned through rapidly to produce its characteristic flickering single-channel behavior. Because β-adrenergic stimulation increases the amount of current, our hypothesis was that in the presence of 8-CPT-cAMP, occupancy of the higher sublevels would be favored. The time spent at each of these subconducting states was different before and after PKA activation, and in the presence of 8-CPT-cAMP, more time was spent at the higher sublevels without any change in subconductance amplitudes (Fig. 5). We also did not

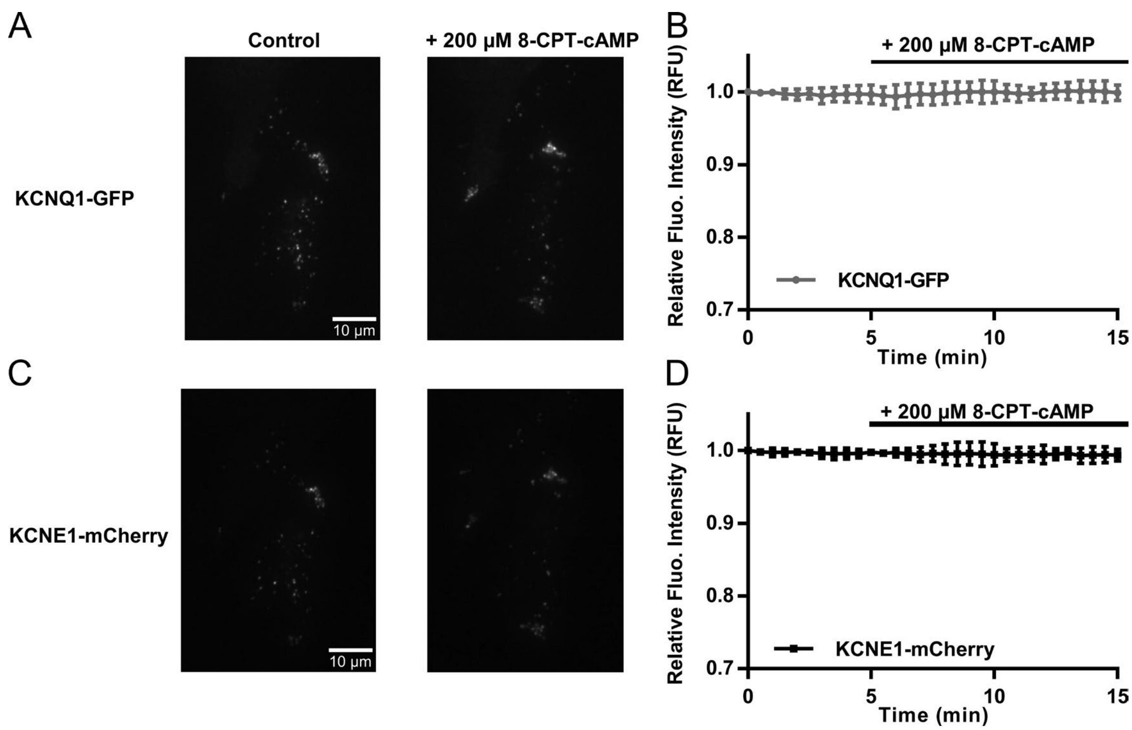

Figure 11. **200 µM 8-CPT-cAMP does not alter overall surface expression of KCNQ1 and KCNE1 subunits in CHO cells.** (A) TIRF images of KCNQ1-GFP before (left) and after (right) addition of 200 µM 8-CPT-cAMP. Images were taken at 0 and 15 min, respectively. (B) Diary plot of change in relative fluorescence units (RFUs) of KCNQ1-GFP with 200 µM 8-CPT-cAMP added at 5 min (n = 7). (C) TIRF images of KCNE1-mCherry before (left) and after (right) addition of 200 µM 8-CPT-cAMP. Images were taken at 0 and 15 min, respectively. (D) Diary plot of change in relative fluorescence intensity of KCNE1-mCherry with 200 µM 8-CPT-cAMP added at 5 min (n = 7). Error bars in B and D show ±SE.

see the appearance of new, larger sublevels in the presence of cAMP (Figs. 3, 4, and 5). The shift of occupancy toward the higher subconducting levels mediated by PKA was accompanied by a 10% decrease in the time spent closed, and together they translate into the well-known increase in macroscopic channel current seen during cAMP administration or β-adrenergic activation. In contrast to the marked effects on latency and subconductance state occupancy, the effects on pore kinetics were minor, with channel closed times and burst kinetics remaining relatively unaffected by 8-CPT-cAMP (Figs. 5 B and 6).

The molecular mechanisms behind the PKA-dependent changes in I_{Ks} current kinetics that we have described are not fully understood. However, it has been suggested that the distance between the Q1 N and C termini shortens once the channel opens (Haitin et al., 2009). Residue Ser[27] is located in the N terminus, and PKA is bound to a complex in the C terminus. Shortening the distance between the N and C termini is thought to be necessary for this phosphorylation to occur (Haitin et al., 2009). How this affects I_{Ks} gating is not understood (Liin et al., 2015), but in the present experiments it appears that most of the effects on the single channels can be explained through actions on the VSD.

Effects of cAMP on the E1R/R4E and S209F channels with augmented VSD function

The E1R/R4E mutant is suggested to possess voltage-independent gating, as the Q1 voltage sensors are suggested to be locked in an upward position (Wu et al., 2010; Zaydman et al., 2014). The S209F KCNQ1 mutant is a VSD gain-of-function mutation that opens at highly hyperpolarized potentials compared with WT, but with much slower or absent deactivation at −80 mV. The increase in Po of S209F compared with WT has been previously reported by Werry et al. (2013), as has a much slower rate of deactivation. These properties are similar to those described for other Q1 gain-of-function mutations (Restier et al., 2008). These mutants allowed us to separate the potential actions of cAMP on pore kinetics from any effects on the VSD, which would already be maximally activated in these mutants. As anticipated, we did not observe a decrease in the number of silent 4-s sweeps, significant decreases in the first latency, or increases in E1R/R4E or S209F channel current amplitudes after 8-CPT-cAMP addition (Figs. 7 and 8). Interestingly, we did still see minor subconductance effects of cAMP on S209F (which presumably retains some ability to show VSD gating), but not on E1R/R4E. It is worth noting that in neither of these mutant channels did we observe an increased appearance of channels in cell-attached patches exposed to cAMP. Perhaps this is caused by trafficking deficiencies between these mutant channels and WT (Eldstrom et al., 2015).

Effects of cAMP on phosphomimetic mutants

Although the main target of phosphorylation for Q1 is Ser^{27}, other phosphorylation sites are also important. Mutating Ser^{27} from a serine to aspartic acid using site-directed mutagenesis recreates the effects of phosphorylation, but to a lesser degree (Kurokawa et al., 2003). As described by Kurokawa et al. (2003), S27D+E1 current densities were twofold higher than WT, and S27D had a slower rate of deactivation when cAMP was present. The $V_{1/2}$ of activation (23.2 ± 4.2 mV in S27D) was hyperpolarized compared with WT (34 mV), but less than with cAMP ($V_{1/2}$ = 4.1 ± 4.3 mV), suggesting that this mutation does not completely recapitulate the hyperpolarizing shift of the $V_{1/2}$ seen in WT.

This is in agreement with our findings. The macropatch data (Fig. S3) show that S27D channels have a more negative $V_{1/2}$ of activation than WT, and that there is still an effect, albeit attenuated, of 8-CPT-cAMP on them. The first latency of S27D is similar to EQ before the addition of cAMP, although the total closed time of S27D+E1 in control is similar to that of EQ plus cAMP. Once 8-CPT-cAMP was added, there was a significant shortening of the first latency (Fig. 9 E and Table 1), but this was proportionally far less (20%) than that observed for either EQ (34%) or Q1+E1 expressed separately (39%). Therefore, this phosphomimetic residue is responsible in part for the shortening of first latency seen when I_{Ks} is exposed to 8-CPT-cAMP, but an additional effect remains. This construct also shows a recruitment of channels upon 8-CPT-cAMP (unpublished data) similar to that of EQ and Q1+E1.

The S27D result suggests that there might be other relevant phosphorylation sites in KCNQ1, and Ser^{92} is another potential N-terminal site (Lopes et al., 2007) that has been shown to increase I_{Ks} current when phosphorylated (Lundby et al., 2013). In the double serine to aspartic acid mutant, S27D/S92D-Q1 channel, changes in macroscopic current amplitude or in the G-V relationship were no longer observed (Fig. 10). At the single-channel level, no significant changes were seen in latency or single-channel conductance, and no obvious differences were seen in subconductance distribution in the raw event histograms. Subconductance analysis of Q1 S27D+E1 patches showed that before 8-CPT-cAMP, this construct occupied the higher open sublevels, much like EQ and Q1+E1 after cAMP (Fig. S4). This suggests that phosphorylation of Ser^{27} is largely responsible for changes in channel Po once activated. However, when 8-CPT-cAMP is present, the time the channel spends closed is further reduced, so other sites like Ser^{92} may be involved in this response, as with the shift in $V_{1/2}$ in macropatches, and the shortening of the first latency that was seen with S27D.

Other than phosphorylation sites in the N terminus of KCNQ1, Yotiao itself is phosphorylated by PKA at a residue in its N terminus, Ser^{43}. Mutation of this serine residue to alanine prevents phosphorylation from occurring and reduces the response to cAMP (Chen et al., 2005). E1, although not a substrate for PKA phosphorylation, is also required for the effect of phosphorylation to occur. Q1 can still be phosphorylated if E1 is not present, but the functional response to phosphorylation is not apparent (Kurokawa et al., 2003). This highlights the importance of E1 in sympathetic regulation of I_{Ks} activity. The E1 C-terminal domain has been suggested to be partly responsible for the I_{Ks} response to phosphorylation. E1-D76N is a LQT-5 mutation in the C terminus that does not respond to cAMP (Kurokawa et al., 2003), and there are a number of other LQT-5 mutations that occur in this region (Splawski et al., 1997; Bianchi et al., 1999).

Trafficking and expression of I_{Ks}

TIRF experiments were done to assess whether the increase in current after cAMP addition was at least in part the result of an increase in trafficking of the channels to the cell membrane. This, however, was not the case, as there appeared to be no overall change in expression levels of Q1 and E1 at the surface of the cell after cAMP exposure (Fig. 11). However, there were clearly areas of local rearrangement of channels (Fig. S7). There are regions from which the channels seem to exit, and areas where there is increased channel density, often where channels are moving toward the edges of the cells. This phenomenon did not seem to be dependent on cAMP, but rather the result of normal turnover of the channel in heterologous cells. This might explain, however, why during single-channel recordings after adding cAMP we sometimes see an increase in the number of channels (Figs. 3 and 4), or even a decrease/complete loss of channel activity (data not depicted).

Others have also shown no increase in Q1 movement to the cell surface upon isoproterenol exposure in COS-7 cells (Wang et al., 2013), although PKA activation is known to alter the rate of trafficking in several channels, such as the cystic fibrosis transmembrane conductance regulator and voltage-gated Na^+ and K^+ channels (Levin et al., 1995; Lehrich et al., 1998; Zhou et al., 2000). $K_v1.1$ channels are affected by PKA activation by two different mechanisms; one where an increase in channel synthesis occurs in response and the second where there is a redistribution of already synthesized channels to the membrane (Levin et al., 1995). It is also worth mentioning that other AKAPs, such as D-AKAP2, have been found to interact with Rab4 and Rab11 proteins and allow for protein recycling regulation (Eggers et al., 2009). In rats, cardiac Na^+ channels have been shown to increase in number at the surface, not directly through PKA modulation, but via the G protein stimulatory α subunit (Lu et al., 1999). The remodeling effect may not be a direct effect on I_{Ks} but an effect on cytoskeleton remodeling that consequently causes relocalization of I_{Ks} channels.

Conclusion

The increase in I_{Ks} current after addition of cAMP is caused by phosphorylation of the VSD at Ser^{27} and other sites, which moves the VSD into more activated states and allows the channels to open more often, more quickly, and to higher sublevels. The direct effects on pore opening and closing are less significant. Our results also suggest that Ser^{27} and Ser^{92} are important phosphorylated residues in this response, but that others may also be of importance. The overall membrane surface expression of I_{Ks} is unchanged by cAMP stimulation, but local rearrangement may occur.

ACKNOWLEDGMENTS

This work was supported by a grant from the Heart and Stroke Foundation of Canada (G-14-0006091), a grant from the Natural Sciences and Engineering Research Council of Canada (RGPIN-2016-05422 to D. Fedida), and a grant from the Fondation pour la Recherche Médicale to E. Balse. M. Westhoff is supported by a Graduate Research Scholarship from the University of British Columbia and was in receipt of a travel scholarship from Mitacs to perform TIRF experiments.

The authors declare no competing financial interests.

Kenton J. Swartz served as editor.

Submitted: 1 December 2016
Accepted: 20 June 2017

REFERENCES

Barhanin, J., F. Lesage, E. Guillemare, M. Fink, M. Lazdunski, and G. Romey. 1996. K(V)LQT1 and lsK (minK) proteins associate to form the I(Ks) cardiac potassium current. *Nature.* 384:78–80. http://dx.doi.org/10.1038/384078a0

Bellocq, C., A.C. van Ginneken, C.R. Bezzina, M. Alders, D. Escande, M.M. Mannens, I. Baró, and A.A. Wilde. 2004. Mutation in the KCNQ1 gene leading to the short QT-interval syndrome. *Circulation.* 109:2394–2397. http://dx.doi.org/10.1161/01.CIR.0000130409.72142.FE

Bianchi, L., Z. Shen, A.T. Dennis, S.G. Priori, C. Napolitano, E. Ronchetti, R. Bryskin, P.J. Schwartz, and A.M. Brown. 1999. Cellular dysfunction of LQT5-minK mutants: Abnormalities of IKs, IKr and trafficking in long QT syndrome. *Hum. Mol. Genet.* 8:1499–1507. http://dx.doi.org/10.1093/hmg/8.8.1499

Boycott, H.E., C.S. Barbier, C.A. Eichel, K.D. Costa, R.P. Martins, F. Louault, G. Dilanian, A. Coulombe, S.N. Hatem, and E. Balse. 2013. Shear stress triggers insertion of voltage-gated potassium channels from intracellular compartments in atrial myocytes. *Proc. Natl. Acad. Sci. USA.* 110:E3955–E3964. http://dx.doi.org/10.1073/pnas.1309896110

Chen, L., J. Kurokawa, and R.S. Kass. 2005. Phosphorylation of the A-kinase-anchoring protein Yotiao contributes to protein kinase A regulation of a heart potassium channel. *J. Biol. Chem.* 280:31347–31352. http://dx.doi.org/10.1074/jbc.M505191200

Chen, Y.H., S.J. Xu, S. Bendahhou, X.L. Wang, Y. Wang, W.Y. Xu, H.W. Jin, H. Sun, X.Y. Su, Q.N. Zhuang, et al. 2003. KCNQ1 gain-of-function mutation in familial atrial fibrillation. *Science.* 299:251–254. http://dx.doi.org/10.1126/science.1077771

Cumbay, M.G., and V.J. Watts. 2004. Novel regulatory properties of human type 9 adenylate cyclase. *J. Pharmacol. Exp. Ther.* 310:108–115. http://dx.doi.org/10.1124/jpet.104.065748

Dessauer, C.W. 2009. Adenylyl cyclase–A-kinase anchoring protein complexes: The next dimension in cAMP signaling. *Mol. Pharmacol.* 76:935–941. http://dx.doi.org/10.1124/mol.109.059345

Dilly, K.W., J. Kurokawa, C. Terrenoire, S. Reiken, W.J. Lederer, A.R. Marks, and R.S. Kass. 2004. Overexpression of β2-adrenergic receptors cAMP-dependent protein kinase phosphorylates and modulates slow delayed rectifier potassium channels expressed in murine heart: Evidence for receptor/channel co-localization. *J. Biol. Chem.* 279:40778–40787. http://dx.doi.org/10.1074/jbc.M406010200

Eggers, C.T., J.C. Schafer, J.R. Goldenring, and S.S. Taylor. 2009. D-AKAP2 interacts with Rab4 and Rab11 through its RGS domains and regulates transferrin receptor recycling. *J. Biol. Chem.* 284:32869–32880. http://dx.doi.org/10.1074/jbc.M109.022582

Eldstrom, J., H. Xu, D. Werry, C. Kang, M.E. Loewen, A. Degenhardt, S. Sanatani, G.F. Tibbits, C. Sanders, and D. Fedida. 2010. Mechanistic basis for LQT1 caused by S3 mutations in the KCNQ1 subunit of IKs. *J. Gen. Physiol.* 135:433–448. http://dx.doi.org/10.1085/jgp.200910351

Eldstrom, J., Z. Wang, D. Werry, N. Wong, and D. Fedida. 2015. Microscopic mechanisms for long QT syndrome type 1 revealed by single-channel analysis of I(Ks) with S3 domain mutations in KCNQ1. *Heart Rhythm.* 12:386–394. http://dx.doi.org/10.1016/j.hrthm.2014.10.029

Gonin, S., G. Deschênes, F. Roger, M. Bens, P.-Y. Martin, J.-L. Carpentier, A. Vandewalle, A. Doucet, and E. Féraille. 2001. Cyclic AMP increases cell surface expression of functional Na,K-ATPase units in mammalian cortical collecting duct principal cells. *Mol. Biol. Cell.* 12:255–264. http://dx.doi.org/10.1091/mbc.12.2.255

Haitin, Y., R. Wiener, D. Shaham, A. Peretz, E.B. Cohen, L. Shamgar, O. Pongs, J.A. Hirsch, and B. Attali. 2009. Intracellular domains interactions and gated motions of I(KS) potassium channel subunits. *EMBO J.* 28:1994–2005. http://dx.doi.org/10.1038/emboj.2009.157

Jost, N., L. Virág, M. Bitay, J. Takács, C. Lengyel, P. Biliczki, Z. Nagy, G. Bogáts, D.A. Lathrop, J.G. Papp, and A. Varró. 2005. Restricting excessive cardiac action potential and QT prolongation: A vital role for IKs in human ventricular muscle. *Circulation.* 112:1392–1399. http://dx.doi.org/10.1161/CIRCULATIONAHA.105.550111

Kurokawa, J., L. Chen, and R.S. Kass. 2003. Requirement of subunit expression for cAMP-mediated regulation of a heart potassium channel. *Proc. Natl. Acad. Sci. USA.* 100:2122–2127. http://dx.doi.org/10.1073/pnas.0434935100

Lehrich, R.W., S.G. Aller, P. Webster, C.R. Marino, and J.N. Forrest Jr. 1998. Vasoactive intestinal peptide, forskolin, and genistein increase apical CFTR trafficking in the rectal gland of the spiny dogfish, *Squalus acanthias*. Acute regulation of CFTR trafficking in an intact epithelium. *J. Clin. Invest.* 101:737–745. http://dx.doi.org/10.1172/JCI803

Levin, G., T. Keren, T. Peretz, D. Chikvashvili, W.B. Thornhill, and I. Lotan. 1995. Regulation of RCK1 currents with a cAMP analog via enhanced protein synthesis and direct channel phosphorylation. *J. Biol. Chem.* 270:14611–14618. http://dx.doi.org/10.1074/jbc.270.24.14611

Li, Y., L. Chen, R.S. Kass, and C.W. Dessauer. 2012. The A-kinase anchoring protein Yotiao facilitates complex formation between adenylyl cyclase type 9 and the IKs potassium channel in heart. *J. Biol. Chem.* 287:29815–29824. http://dx.doi.org/10.1074/jbc.M112.380568

Liin, S.I., R. Barro-Soria, and H.P. Larsson. 2015. The KCNQ1 channel—Remarkable flexibility in gating allows for functional versatility. *J. Physiol.* 593:2605–2615. http://dx.doi.org/10.1113/jphysiol.2014.287607

Lopes, C.M., J.I. Remon, A. Matavel, J.L. Sui, I. Keselman, E. Medei, Y. Shen, A. Rosenhouse-Dantsker, T. Rohacs, and D.E. Logothetis. 2007. Protein kinase A modulates PLC-dependent regulation and PIP2-sensitivity of K+ channels. *Channels (Austin).* 1:124–134. http://dx.doi.org/10.4161/chan.4322

Lu, T., H.C. Lee, J.A. Kabat, and E.F. Shibata. 1999. Modulation of rat cardiac sodium channel by the stimulatory G protein alpha subunit. *J. Physiol.* 518:371–384. http://dx.doi.org/10.1111/j.1469-7793.1999.0371p.x

Lundby, A., M.N. Andersen, A.B. Steffensen, H. Horn, C.D. Kelstrup, C. Francavilla, L.J. Jensen, N. Schmitt, M.B. Thomsen, and J.V. Olsen. 2013. In vivo phosphoproteomics analysis reveals the cardiac targets of β-adrenergic receptor signaling. *Sci. Signal.* 6:rs11. http://dx.doi.org/10.1126/scisignal.2003506

Marx, S.O., J. Kurokawa, S. Reiken, H. Motoike, J. D'Armiento, A.R. Marks, and R.S. Kass. 2002. Requirement of a macromolecular signaling complex for beta adrenergic receptor modulation of the KCNQ1-KCNE1 potassium channel. *Science.* 295:496–499. http://dx.doi.org/10.1126/science.1066843

Moss, A.J., P.J. Schwartz, R.S. Crampton, D. Tzivoni, E.H. Locati, J. MacCluer, W.J. Hall, L. Weitkamp, G.M. Vincent, A. Garson Jr., et al. 1991. The long QT syndrome. Prospective longitudinal study of 328 families. *Circulation.* 84:1136–1144. http://dx.doi.org/10.1161/01.CIR.84.3.1136

Murray, C.I., M. Westhoff, J. Eldstrom, E. Thompson, R. Emes, and D. Fedida. 2016. Unnatural amino acid photo-crosslinking of the IKs channel complex demonstrates a KCNE1:KCNQ1 stoichiometry of up to 4:4. *eLife.* 5:e11815. http://dx.doi.org/10.7554/eLife.11815

Piggott, L.A., A.L. Bauman, J.D. Scott, and C.W. Dessauer. 2008. The A-kinase anchoring protein Yotiao binds and regulates adenylyl cyclase in brain. *Proc. Natl. Acad. Sci. USA.* 105:13835–13840. http://dx.doi.org/10.1073/pnas.0712100105

Restier, L., L. Cheng, and M.C. Sanguinetti. 2008. Mechanisms by which atrial fibrillation-associated mutations in the S1 domain of KCNQ1 slow deactivation of IKs channels. *J. Physiol.* 586:4179–4191. http://dx.doi.org/10.1113/jphysiol.2008.157511

Sanguinetti, M.C., and N.K. Jurkiewicz. 1990. Two components of cardiac delayed rectifier K+ current. Differential sensitivity to block by class III antiarrhythmic agents. *J. Gen. Physiol.* 96:195–215. http://dx.doi.org/10.1085/jgp.96.1.195

Sanguinetti, M.C., M.E. Curran, A. Zou, J. Shen, P.S. Spector, D.L. Atkinson, and M.T. Keating. 1996. Coassembly of K(V)LQT1 and minK (IsK) proteins to form cardiac I(Ks) potassium channel. *Nature.* 384:80–83. http://dx.doi.org/10.1038/384080a0

Schwarzer, S., G.I. Mashanov, J.E. Molloy, and A. Tinker. 2013. Using total internal reflection fluorescence microscopy to observe ion channel trafficking and assembly. *Methods Mol. Biol.* 998:201–208. http://dx.doi.org/10.1007/978-1-62703-351-0_15

Silva, J., and Y. Rudy. 2005. Subunit interaction determines IKs participation in cardiac repolarization and repolarization reserve. *Circulation.* 112:1384–1391. http://dx.doi.org/10.1161/CIRCULATIONAHA.105.543306

Splawski, I., M. Tristani-Firouzi, M.H. Lehmann, M.C. Sanguinetti, and M.T. Keating. 1997. Mutations in the hminK gene cause long QT syndrome and suppress IKs function. *Nat. Genet.* 17:338–340. http://dx.doi.org/10.1038/ng1197-338

Splawski, I., J. Shen, K.W. Timothy, M.H. Lehmann, S. Priori, J.L. Robinson, A.J. Moss, P.J. Schwartz, J.A. Towbin, G.M. Vincent, and M.T. Keating. 2000. Spectrum of mutations in long-QT syndrome genes. KVLQT1, HERG, SCN5A, KCNE1, and KCNE2. *Circulation.* 102:1178–1185. http://dx.doi.org/10.1161/01.CIR.102.10.1178

Stengl, M., P.G. Volders, M.B. Thomsen, R.L. Spätjens, K.R. Sipido, and M.A. Vos. 2003. Accumulation of slowly activating delayed rectifier potassium current (IKs) in canine ventricular myocytes. *J. Physiol.* 551:777–786. http://dx.doi.org/10.1113/jphysiol.2003.044040

Takumi, T., H. Ohkubo, and S. Nakanishi. 1988. Cloning of a membrane protein that induces a slow voltage-gated potassium current. *Science.* 242:1042–1045. http://dx.doi.org/10.1126/science.3194754

Terrenoire, C., C.E. Clancy, J.W. Cormier, K.J. Sampson, and R.S. Kass. 2005. Autonomic control of cardiac action potentials: Role of potassium channel kinetics in response to sympathetic stimulation. *Circ. Res.* 96:e25–e34. http://dx.doi.org/10.1161/01.RES.0000160555.58046.9a

Tristani-Firouzi, M., and M.C. Sanguinetti. 1998. Voltage-dependent inactivation of the human K+ channel KvLQT1 is eliminated by association with minimal K+ channel (minK) subunits. *J. Physiol.* 510:37–45. http://dx.doi.org/10.1111/j.1469-7793.1998.037bz.x

Wang, Q., M.E. Curran, I. Splawski, T.C. Burn, J.M. Millholland, T.J. VanRaay, J. Shen, K.W. Timothy, G.M. Vincent, T. de Jager, et al. 1996. Positional cloning of a novel potassium channel gene: KVLQT1 mutations cause cardiac arrhythmias. *Nat. Genet.* 12:17–23. http://dx.doi.org/10.1038/ng0196-17

Wang, Y., D.P. Zankov, M. Jiang, M. Zhang, S.C. Henderson, and G.-N. Tseng. 2013. [Ca2+]i elevation and oxidative stress induce KCNQ1 protein translocation from the cytosol to the cell surface and increase slow delayed rectifier (IKs) in cardiac myocytes. *J. Biol. Chem.* 288:35358–35371. http://dx.doi.org/10.1074/jbc.M113.504746

Werry, D., J. Eldstrom, Z. Wang, and D. Fedida. 2013. Single-channel basis for the slow activation of the repolarizing cardiac potassium current, I(Ks). *Proc. Natl. Acad. Sci. USA.* 110:E996–E1005. http://dx.doi.org/10.1073/pnas.1214875110

Wit, A.L., B.F. Hoffman, and M.R. Rosen. 1975. Electrophysiology and pharmacology of cardiac arrhythmias. IX. Cardiac electrophysiologic effects of beta adrenergic receptor stimulation and blockade. Part C. *Am. Heart J.* 90:795–803. http://dx.doi.org/10.1016/0002-8703(75)90471-8

Wu, D., K. Delaloye, M.A. Zaydman, A. Nekouzadeh, Y. Rudy, and J. Cui. 2010. State-dependent electrostatic interactions of S4 arginines with E1 in S2 during Kv7.1 activation. *J. Gen. Physiol.* 135:595–606. http://dx.doi.org/10.1085/jgp.201010408

Yamamura, H., Y. Suzuki, and Y. Imaizumi. 2015. New light on ion channel imaging by total internal reflection fluorescence (TIRF) microscopy. *J. Pharmacol. Sci.* 128:1–7. http://dx.doi.org/10.1016/j.jphs.2015.04.004

Zaydman, M.A., M.A. Kasimova, K. McFarland, Z. Beller, P. Hou, H.E. Kinser, H. Liang, G. Zhang, J. Shi, M. Tarek, and J. Cui. 2014. Domain-domain interactions determine the gating, permeation, pharmacology, and subunit modulation of the IKs ion channel. *eLife.* 3:e03606. http://dx.doi.org/10.7554/eLife.03606

Zhou, J., J. Yi, N. Hu, A.L. George Jr., and K.T. Murray. 2000. Activation of protein kinase A modulates trafficking of the human cardiac sodium channel in *Xenopus* oocytes. *Circ. Res.* 87:33–38. http://dx.doi.org/10.1161/01.RES.87.1.33